Interpreting the seasonal environmental history recorded by Arctic bivalves

Vihtakari Mikko[1,2,3,*], Ambrose William G. Jr.[2,4], Renaud Paul E.[2,5], Locke William L. V[4], Carroll Michael L.[2], Berge Jørgen[1,5], Clarke Leon J.[6], Cottier Finlo[7], Hop Haakon[3]

1 Department of Arctic and Marine Biology, UiT The Arctic University of Norway, N-9037 Tromsø, Norway
2 Akvaplan-niva, Fram Centre, N-9296 Tromsø, Norway
3 Norwegian Polar Institute, Fram Centre, N-9296 Tromsø, Norway
4 Department of Biology, Bates College, Lewiston, Maine 04240, USA
5 University Centre in Svalbard, N-9171 Longyearbyen, Norway
6 School of Science and the Environment, Faculty of Science and Engineering, Manchester Metropolitan University, Manchester, M1 5GD, UK
7 Scottish Association for Marine Science, Scottish Marine Institute, Oban, Argyll PA37 1QA, UK
∗ **E-mail: mikko.vihtakari@gmail.com**

Keywords: *Serripes groenlandicus*; *Ciliatocardium ciliatum*; Laser-Ablation Inductively-Coupled-Plasma Mass-Spectrometry; paleoclimatology; paleoceanography; bivalve mollusk shells; *in situ* analyses; shell mineralogy

Abstract

Understanding rapid climate change in the Arctic and its ecosystem implications requires more information on the environment at temporal resolutions and time-periods not available from the instrumental records. Such information can be acquired through geochemical proxy records, but sub-annual records are rare in the literature. We analyzed shell material of bivalve mollusks (*Serripes groenlandicus* and *Ciliatocardium ciliatum*) that were placed on oceanographic moorings for one year in two Arctic fjords to assess the potential use of shell elemental ratios as environmental proxies. Li/Ca, Mg/Ca, Li/Mg, Mn/Ca, Sr/Ca, Mo/Ca and Ba/Ca were determined using Laser-Ablation Inductively-Coupled-Plasma Mass-Spectrometry. The mooring exposure, combined with previously derived sub-annual shell growth models, allowed us to relate the elemental ratio patterns to oceanographic data (temperature, salinity, and fluorescence) collected by instruments attached to the moorings. Shell Ba/Ca profiles were characterized by abrupt peaks occurring 11 to 81 days after the phytoplankton bloom, as indicated by the seawater fluorescence index. Li/Ca and Mg/Ca values exhibited a logarithmic relationship with shell growth rate, indicated by marginal R^2 of 0.43 and 0.30, respectively. These ratios were also linearly related to temperature, with marginal R^2 of 0.15 and 0.17, respectively. Mn/Ca and Sr/Ca ratios exhibited variability among individuals and their temporal pattern was likely controlled by several unidentified factors. Mo/Ca patterns within the shells did not demonstrate meaningful correlations with any mooring instrument data. Our results reflect complex relationships between elemental ratios, bivalve metabolism, methodological limitations, and synchronized environmental processes suggesting that none of the studied elemental ratios can be used as all-encompassing proxies of seawater temperature, salinity, paleoproductivity, or shell

growth rate. Despite this, Ba/Ca and Li/Ca can likely be used as sub-annual temporal anchors in further studies, as the deposition of these elements likely occurred simultaneously within each fjord.

1 Introduction

The annual sea ice cover over the Arctic Ocean has declined by approximately 20 % since the industrial revolution [data from Figure 4.3a in 1] with an accelerating rate over the last decade [2]. Such a reduction in sea-ice cover, together with other anthropogenic perturbations, is expected to cause dramatic changes in Arctic marine ecosystems [2, 3]. Understanding and anticipating these rapid changes requires information about the past climate at sufficient temporal resolution and over longer time-periods than that usually provided by instrumental records [4]. Such knowledge can be acquired by interpretation of geochemical proxy records, which can represent long time scales [4–6]. Whereas records of environmental changes at longer than decadal time-scales may indicate correlative relationships between climatic and biological patterns, combining environmental and biotic data at sub-annual scales can help identify the ecological mechanisms through which climate regulates biotic processes. Unfortunately, there are few sub-seasonal high-resolution records presented in the literature due to a paucity of available data.

Shells of many filter-feeding bivalve mollusks are promising geochemical proxy archives due to: 1) largely sedentary nature of bivalves, meaning that individuals record temporal rather than spatial variability in seawater conditions; 2) distribution of bivalves across a wide variety of habitats and latitudes [7]; 3) representation of bivalve shells in the geological record [7–10]; 4) longevity of bivalves allowing longer than decadal proxy records per individual [11–13]; and 5) regular growth patterns in bivalve shells that can be used to develop growth chronologies [14–17]. Two common circumpolar bivalve species, the Greenland cockle (*Serripes groenlandicus* Mohr, 1786) and the hairy cockle (*Ciliatocardium ciliatum* Fabricius, 1780), have been used as environmental and climatic indicators in the previous studies [18–22]. They are long lived species forming an aragonitic shell [23–25] with prominent annual growth lines deposited during a slow winter shell growth period that is regulated by food availability [17, 19, 26]. Their shell growth is further affected by temperature and often correlates with large scale climatic drivers over annual to decadal scales [18, 20–22].

In theory, the environmental information stored in bivalve shells can be used to hind-cast seawater conditions with a sub-annual resolution based on geochemical proxies, such as element-to-calcium ratios, that are sampled along chronologically deposited shell material [27–29]. Several elemental ratios, such as Li/Ca [30, 31], Mg/Ca [32, 33], and Sr/Ca [34], have been suggested as proxies of seawater temperature in bivalve shells, but these ratios are often affected by metabolic and kinetic processes, and thus may be used as temperature proxies only for specific cases when shell growth rate and seawater temperature are strongly intercorrelated [35, 36]. Lithium to magnesium ratio could potentially be used to tease apart the metabolic effects in Li/Ca and Mg/Ca [37]. The ratios of barium, manganese, molybdenum, and lithium to calcium have been suggested as proxies of pelagic productivity [31, 38–40]. Barium to calcium provides one of the most consistent elemental ratio signals in bivalve shells: Ba/Ca profiles are characterized by a flat background signal that is periodically interrupted by sharp peaks in a wide range of species

across various habitats and latitudes [24, 38, 39, 41–48]. In addition to potentially representing variability in primary productivity, Ba/Ca may indicate ambient seawater concentrations [49]. In contrast, manganese is often associated with shell precipitation rate and may also be influenced by seawater redox conditions, and therefore shows variable patterns depending on species [50–54]. Molybdenum, on the other hand, may be incorporated through diet, making Mo/Ca a potential proxy of paleoproductivity [40, 49].

Consequently, the development of elemental ratios in bivalve shells as environmental proxies could be valuable, especially in the Arctic where instrumental records are short or interrupted and climate change is rapid [55]. Elemental ratio proxies in bivalve shells are, however, complicated by metabolism as calcium carbonate mineralization does not occur directly from seawater, but takes place in a chemically controlled space; the extrapallial cavity [56–58]. Interpretation of these geochemical proxies is further complicated by shell growth rate, which varies through the year [17] and appears to influence some element ratios [36]. Consequently, understanding the sub-annual growth patterns is a fundamental prerequisite for using any shell-based proxy at sub-annual resolution. Very few studies, and none in the Arctic, have been able to relate elemental ratios measured within bivalve shells to seawater parameters data recorded at the growth location with sub-annual resolution.

In this study, we examine minor and trace elemental ratios within the shells of *S. groenlandicus* and *C. ciliatum*, and assess their potential use as environmental proxies. We deployed these bivalves on moorings in two oceanographically contrasting fjords in Svalbard for one year [17, 26]. The bivalve deployment combined with previously obtained sub-annual growth models [17] allowed us to relate the elemental ratio patterns to the oceanographic data recorded by mooring instrumentation. We aimed to examine whether: 1) Li/Ca, Ba/Ca, Mn/Ca or Mo/Ca could be used as proxies of primary productivity as has been suggested by other studies, 2) Li/Ca, Mg/Ca, Li/Mg or Sr/Ca could be used as proxies of temperature or shell growth rate, and 3) any of the above mentioned elemental ratios were deposited simultaneously in different individuals indicating that they could be used as sub-annual chronological markers in the studied species.

2 Materials and Methods

2.1 Study design

A suite of element (Li, Mg, Mn, Sr, Mo, and Ba) to calcium ratios was determined for sub-annual patterns in shells of two bivalve species (*Serripes groenlandicus* and *Ciliatocardium ciliatum*) deployed on oceanographic moorings for one year during the periods September 2007–2008 and September 2009–2010 in two fjords on Svalbard: Kongsfjorden and Rijpfjorden. These two fjords are oceanographically different. Kongsfjorden is an Atlantic water-influenced open fjord, whereas Rijpfjorden is a fjord with a sill (depth 100-200 m) that is influenced mainly by Arctic water masses [59–62]. Kongsfjorden was ice-free throughout the field deployment with the exception of occasional drift ice, whereas Rijpfjorden was covered by sea ice for 8 months (January 21–September 16) in 2007–2008 [63], and for 5 months (February 15–July 21) in 2009-2010 [17]. The bivalve deployment on moorings is described in detail by Ambrose Jr *et al.* [26] and Vihtakari *et al.* [17]. In brief, bivalves were collected from the western Barents Sea in August 2007 and

from Svalbardbanken in August 2009. They were held in flow-through seawater tanks for 1–4 weeks at the University Centre in Svalbard and incubated in seawater with 125 mg L^{-1} of calcein dye for 24 h immediately before they were placed in 7 mm mesh plastic cages (hereafter baskets) on the oceanographic moorings. The calcein mark was used as an absolute time marker of deployment and was identified in sectioned shells using fluorescent imaging [see 17]. During 2009-2010, the bivalves were deployed to two water depths, 15 m (basket A) and 25 m (basket B), while in 2007-2008 they were deployed only to 25 m (Table 1). The bivalves were deployed in September each year and recovered one year later.

Bivalves collected from the moorings were sacrificed and shells then were embedded in epoxy resin [as described in 26]. Embedded shells were cut into thick sections along the maximum growth axis, as described in Vihtakari *et al.* [17], and the thick sections were polished to a thickness of 2.0 ± 0.1 mm. These thick sections then were transferred to a clean room, where they were rinsed and brushed in Milli-Q water, sonicated for 5 min and rinsed again. Finally, the thick sections were left to dry overnight before they were analyzed using Laser-Ablation Inductively-Coupled-Plasma Mass-Spectrometry (hereafter LA-ICP-MS). Eleven shells were further analyzed for *in situ* $\delta^{18}O$ values using secondary ion mass spectrometry (SIMS) to determine sub-annual growth models [see 17]. Measured element ratio patterns determined for nine shells that demonstrated adequate growth models were compared to weekly averages of seawater temperature, salinity and fluorescence index records obtained from mooring instruments located adjacent to bivalve baskets (Table 2, see 17 for details).

2.2 Elemental ratio analyses

LA-ICP-MS [64] was conducted at the Plasma Mass Spectrometry Facility, Woods Hole Oceanographic Institute (MA, US), using a Thermo-Finnigan Element2 HR-ICP-MS coupled to a New Wave Laser UP 193 nm excimer laser ablation system. A sequence of holes was ablated along the middle of the shell thick section from the outer margin to the calcein line [see 17] using 95 s dwell time, 10 Hz repetition rate and 90% output power. The analysis was conducted in 2009 for 2007-2008 deployment specimens and in 2011 for 2009-2010 deployment individuals. Magnesium (^{25}Mg), calcium (^{48}Ca), manganese (^{55}Mn), strontium (^{88}Sr) and barium (^{138}Ba) were analyzed in both years. Molybdenum (^{98}Mo) and lithium (^{7}Li) were added to the analysis for 2009-2010 samples. Due to the low concentration of Mo in the $CaCO_3$ matrix, 2009-2010 shells had a larger ablation crater size [$\bar{x} = 87.5 \pm 0.7$ µm (SE), n = 612] compared to 2007-2008 samples [$\bar{x} = 42.0 \pm 0.3$ µm (SE), n = 311]. The distance between laser holes [$\bar{x} = 104.1 \pm 14.3$ (SD) µm] was kept constant between sessions and samples, and therefore the number of ablation holes varied between 17 and 64 per analyzed shell depending on the length of annual growth increment.

The signal intensity (counts per second) of the analyzed elements was monitored in an Element2 low resolution mode during the LA-ICP-MS analyses. The recording of element signal intensity was started approximately 10 s after initiating the laser ablation to clean the shell surface of debris and to ensure that the ablation plume material had reached the ICP-MS. An estimated value for each element was generated by averaging 50 signal intensity measurements during the peak of material flow. Nitric acid (5 % HNO_3) was used as a blank, ensuring a constant flow of the acid into the ICP-MS. Every tenth sample analyzed was a blank. The

moving average of blanks was calculated and subtracted from the data. Since the analyzed shell matrix was predominantly aragonite [23, 25], ^{48}Ca was used as an internal standard by normalizing all other elements to Ca concentration [65]. Two standards, Japanese Certified Reference Material or "JpnCRM" [66] and FEBS-1 [67], were run as every tenth and twentieth sample, respectively. These standards were used to correct for instrument drift and to calibrate elemental ratios to cover all isotopes. FEBS-1 was used for Mn/Ca and Li/Ca and JpnCRM for the other elemental ratios. The reference materials did not have a certified value for Mo. Therefore, Mo/Ca concentrations are given as percentage of Mo/Ca maximum for each shell and comparison of absolute Mo/Ca values was not possible

2.3 Datasets and statistical analyses

The position of the LA-ICP-MS holes was related to sub-annual growth lines and a measurement axis that was related to the historical location of the shell margin using ImageJ [68] and sclero package [69] for R software [70], as described in Vihtakari *et al.* [17]. The method also allowed a spatial estimation of averaging error [71, 72]. Resulting LA-ICP-MS sample distances are therefore expressed as mm from deployment (i.e. the calcein mark) along the measurement axis, together with minimum and maximum extents for each LA-ICP-MS hole (Figures S1–S6).

Growth models for nine shells (three from each basket: KB, RA and RB, Table 1), based on estimated daily growth trajectories for SIMS δ^{18}O centroids (Figure 9 in 17), allowed comparison of elemental ratio data to mooring instrument data (temperature, fluorescence index and salinity) and modeled growth rate. The estimated temporal extent sampled by each LA-ICP-MS hole was used to calculate average growth rate, temperature, salinity, and fluorescence index values that were used as predictor variables in consequent regression models. The averages were calculated using daily values. The relationship between element ratios (response variable in all models) and shell growth rate was logarithmic, and therefore growth rates were log-transformed before analyses.

Linear mixed-effect regression models (LMMs) were used to examine the overall relationships in the dataset by using samples as random effects, assuming a random intercept and a constant slope (see Table S3 and Text S1 for definitions of the models). In order to examine the overall variance of each elemental ratio explained by each predictor variable, LMMs were run separately with each non-transformed predictor variable (Model 1; Table S3). Marginal and conditional R^2 values for LMMs for these models were calculated using MuMIn package [73] for R [70] and the method described by Johnson [74]. Marginal R^2 values were used as a measure of overall variance explained by each response variable and to examine whether the proxy relationship was constant among samples. To examine the overall relative importance of each predictor variable and the direction of the linear relationship, all predictor variables were combined as fixed effects into a same LMM (Model 2; Table S3). Response variables were log-transformed, and predictor variables centered to their means and scaled to their standard deviations before running Model 2. The fixed effects (effects of each predictor variable to an elemental ratio) then were scaled to the maximum absolute value of 95% confidence intervals resulting to a measure of relative effect for each fixed effect. Linear mixed-effect models were calculated using the nlme package [75]. The variability in relationships between response and predictor variables among individual samples was examined using linear regression models fitted for each sample, response variable

and predictor variable separately (Model 3; Table S3).

Coefficients of variation (CV) for minimum and maximum elemental ratios over the mooring deployment were used to assess among individual consistency of elemental ratios using all analyzed shells over two deployment periods (n = 30, Table 1). Correlations between elemental ratios and predictor variables for regression models were examined using principal component analysis [76] calculated on correlation matrices averaged over samples using Fisher z-transformation [77–79]. These correlation matrices are presented in Table S4.

3 Results

3.1 Oceanographic conditions in the fjords

Kongsfjorden experienced warmer temperatures in 2007-2008 than in 2009-2010 (Figure 1): The autumn (September to December) temperatures in Kongsfjorden were on average 1.0 °C higher in 2007 compared to 2009, the winter (January to April) temperatures 1.7 °C warmer, and the spring/summer (May to September) temperatures 2.6 °C warmer in 2008 compared to 2010. In contrast, temperature differences between years varied in Rijpfjorden: The autumn (September to November) temperatures in Rijpfjorden were also on average 1.0 °C higher in 2007 compared to 2009, the winter (December to May) temperatures were almost equal between deployment years, but the summer temperatures were on average 2.4 °C lower in 2008 compared to 2010. In Kongsfjorden, temperature began to increase in May in both years. In 2007-2008, temperature remained above zero, while in the winter of 2009-2010, temperature was generally below zero. Temperature was recorded at two depths (15 and 25 m) in 2009-2010. Temperature differences between depths were generally small, except during the summer stratification period, when temperature at 15 m was approximately 1 °C higher than at 25 m. Rijpfjorden experienced temperatures close to -1.7 °C from January until July (6 months) in 2007-2008 and from January until June (5 months) in 2009-2010. Temperature rose abruptly in mid-July 2010, whereas in 2008 it started increasing in mid-May, but did not exceed 0 °C. In 2009-2010, temperatures were similar at both measured depths until late August, when the surface layer cooled by approximately 3 °C relative to the deeper (25 m) layer.

In both fjords, the fluorescence index (FLI) was close to zero prior to a dramatic increase during the spring (Figure 1). The first fluorescence peak occurred later (mid-June to mid-July) in Rijpfjorden than in Kongsfjorden (mid-May to beginning of June). Salinity was relatively stable in Kongsfjorden, with a range between 33.3 and 35.0 (Figure 1). Rijpfjorden experienced variable salinity regime, related to melt water from sea ice, from July to December. Salinity varied more in 2009-2010 (34.6-30.6) than in 2007-2008 (34.3-31.7), and was most variable at the shallow baskets (15 m).

3.2 Patterns in element ratio profiles

Lithium to calcium ratios were consistently lower during winter and increased after the winter growth band in all studied shells (Figures 2, S3–S6). The increase occurred simultaneously with increased growth rate in growth modeled shells (Figures 2 and S7). Minimum Li/Ca was 13.9 ± 0.3 (SE, n = 22) $\mu mol\,mol^{-1}$ on average (Table 3). The Li/Ca minimum was deposited

sometime between October and late May in Kongsfjorden and between October and mid-July in Rijpfjorden (Figure 2). Coefficient of variation for minimum Li/Ca values varied between 7.5 and 14.1 % among baskets and was higher than that for maximum values (Table 3). The maximum values were 21.6 ± 0.3 (SE, n = 22) on average, and were estimated to occur July to early September in Kongsfjorden and mid-July to early August in Rijpfjorden (Figure 2).

Magnesium to calcium ratios were at their lowest during the winter growth band and increased immediately after or towards the end of the winter growth period in most analyzed shells (Figures 2 and S1–S6). Three shells deployed to Rijpfjorden in 2007, however, did not demonstrate clear seasonal Mg/Ca fluctuations (Figure S2). The strongest increase in Mg/Ca values occurred during spring together with increased growth rate (Figures 2 and S8). After reaching the maximum in July to mid-August in Kongsfjorden and in late July to late August in Rijpfjorden, Mg/Ca values decreased slightly until the end of the deployment period (Figure 2). Maximum Mg/Ca values ranged between 1.04 and 4.15 $\mathrm{mmol\,mol^{-1}}$ being generally higher in 2009-2010 than in 2007-2008 (Table 3). Minimum Mg/Ca values ranged between 0.39 and 1.70 $\mathrm{mmol\,mol^{-1}}$ and were not obviously different among years. Coefficient of variation for Mg/Ca minimum and maximum values was higher than that for Li/Ca (Table 3).

Manganese to calcium values exhibited variable patterns, but were also characterized by peaks deposited during the translucent summer growth period in 24 of 30 analyzed shells (Figure S1–S6). These peaks were deposited sometime between late May and August in Kongsfjorden, and between early July and early August in Rijpfjorden occurring one to 70 days after the fluorescence peak (Table 4 and Figure 2). Low Mn/Ca values were deposited during the winter growth band from January until the end of the winter growth band (Figure S9). Average maximum manganese values ranged between 1.31 and 8.52 $\mathrm{\mu mol\,mol^{-1}}$ (Table 3). Maximum Mn/Ca values within baskets showed high variability as illustrated by coefficient of variation (Table 3). Average minimum Mn/Ca values ranged between 0.16 and 0.75 $\mathrm{\mu mol\,mol^{-1}}$ among baskets, and coefficient of variation was high (Table 3). Average minimum and maximum values were lower in 2009-2010 (Table 3).

Individuals within baskets demonstrated considerable variability with respect to Sr/Ca profiles (Figures 2, S1–S6). Minimum values were deposited before the winter growth band in 3 samples, during the winter growth in 4 samples, and after the winter growth in 23 samples. Furthermore, maximum Sr/Ca values occurred before, during and after the winter growth band in 7, 7, and 16 samples, respectively (Figures S1–S6). Minimum Sr/Ca values were deposited between May and August in two growth modeled *S. groenlandicus* from Kongsfjorden and between October and March in the growth modeled *C. ciliatum* specimen (Figures 2 and S10). In Rijpfjorden, the minimum values were deposited between July and mid-August in seven shells and between April and mid-July in one *S. groenlandicus* specimen (Figure 2). Maximum Sr/Ca values in growth modeled shells from Kongsfjorden were deposited at the end of the mooring deployment in mid-September, whereas Rijpfjorden shells showed more variability with maximum values occurring in the beginning of the mooring deployment (September to December) as well as towards the end of the mooring deployment (August to September, Figure 2). Coefficient of variation for minimum and maximum Sr/Ca values was lower than those for Mg/Ca (Table 3). Minimum Sr/Ca value was 1.32 ± 0.04 $\mathrm{mmol\,mol^{-1}}$ (SE, n = 30) on average and maximum value 2.37 ± 0.09 $\mathrm{mmol\,mol^{-1}}$ (SE, n = 30).

Molybdenum to calcium ratios were at their highest during or before the winter growth

band in all shells analyzed for Mo/Ca (2009-2010) and the ratios decreased after the end of the growth check (Figures 2, S3–S6). After the minimum Mo/Ca, which occurred between mid-April and September in Kongsfjorden and between July and August in Rijpfjorden, Mo/Ca values increased again until the end of the mooring exposure (mid-September 2010, Figures 2 and S11). Maximum Mo/Ca values were measured at the beginning of the mooring deployment (September to April, Figure 2).

Barium to calcium profiles were characterized by abrupt unimodal peaks (maximum values = 3.1-76.1 µmol mol^{-1}, $\bar{x}$ = 20.0 µmol mol^{-1}, Table 5) that were differentiated from low Ba/Ca background levels (0.43–2 µmol mol^{-1}, $\bar{x}$ = 1 µmol mol^{-1}, Figures 2, S1–S6). The peaks appeared annually, occurring subsequent to the winter growth band in 27 of 30 analyzed shells (Figures S1–S6). A distinct barium peak was not present in two *C. ciliatum* from 2007-2008 deployed in the 25 m basket in Rijpfjorden (Figure S2) and one *C. ciliatum* from 2009-2010 deployed in the 15 m basket in Kongsfjorden (Figure S3). In 2009-2010 samples, the Ba maxima were considerably lower in the 25 m basket in Rijpfjorden compared to other baskets (RB in Table 3 and Figure S6). Barium peak values were not consistent within a basket as indicated by high coefficient of variation (Table 3). The minimum Ba/Ca values were associated with a lower within basket variability than the maximum values (Table 3). Barium peaks in Kongsfjorden were estimated to occur between June and mid-August, 18 to 100 days after the fluorescence peak (Table 5). Further, Ba/Ca peak values were deposited in July in Rijpfjorden occurring 11 to 36 days after the first peak in fluorescence index (Table 5).

3.3 Correlations between element ratios, growth rates and mooring instrument data

Li/Ca and Mg/Ca covaried within 2009-2010 shells as indicated by arrows pointing approximately to the same direction in the PCA plot (Figure 3B) and high correlation coefficients (r_z = 0.78, r = 0.13–0.92; Table S4). Similar correlations between element ratios were evident for Sr/Ca and Mo/Ca in 2009-2010 (Figure 3B, r_z = 0.59, r = −0.69–0.99), Mn/Ca and Ba/Ca – especially in the growth modeled shells (Figure 3C, r_z = 0.50, r = −0.02–0.78), and Mg/Ca and Mn/Ca in 2007-2008 shells (Figure 3A, r_z = 0.38, r = −0.31–0.78). Further, Mg/Ca and Li/Mg were strongly negatively correlated in 2009-2010 shells as demonstrated by arrows pointing to opposite directions in the PCA plot (Figure 3B, r_z = −0.92, r = −0.99 – −0.60). Also Li/Ca and Li/Mg, Mg/Ca and Mo/Ca, and Li/Ca and Mo/Ca were negatively correlated (Table S4). Temperature and salinity were negatively correlated (r_z = −0.71, r = −0.86–0.57), whereas temperature yielded positive correlations with fluorescence (r_z = 0.48, r = 0.34–0.67) and logarithm of shell growth rate (r_z = 0.43, r = 0.22–0.66, Figure 3D).

Overall, logarithm of growth rate was the best explanatory factor for element ratio variability in growth modeled shells (Figure 4A). Coefficient of determination (R^2) for individual samples ranged between 0.19 and 0.75 for the regression between Li/Ca and growth rate, between 0.30 and 0.59 for Mg/Ca, between 0.11 and 0.24 for Li/MG, and between 0.01 and 0.87 for Mn/Ca (Table S2). Also Sr/Ca exhibited significant regressions with growth rate, but these relationships varied from positive to negative (Table S2). Temperature yielded significant regressions with Li/Ca, Mg/Ca, Li/Mg, and Sr/Ca (Table S2), but in the majority of samples these regressions were not as strong as those for logarithm of growth rate (Figure 4A). The temperature

relationships for Li/Ca, Mg/Ca and Li/Mg were relatively consistent among samples, although associated with large residual standard error (Tables S1–S2).

4 Discussion

Barium, manganese, molybdenum, and lithium to calcium ratios have previously been related to primary production [31, 38–40] (Section 4.1). Although Mn/Ca and Ba/Ca exhibited patterns that resembled the patterns in the fluorescence index (Figure 2), which was used as a proxy of primary production, the differences in peak heights among samples from the same basket suggested that these element ratios were also affected by other processes and could not be used as straightforward proxies of primary production (Tables 3–5; see Section 4.1). Despite this, Ba peaks were deposited likely at the same in a basket, but the timing varied between baskets occurring 11 to 81 days after the phytoplankton bloom (Figure 2, Table 5, Section 4.3). Ba/Ca could potentially be related to dissolved or particular Ba in ambient seawater. Mo/Ca and Li/Ca did not exhibit patterns that could have been linked to primary production (Figure 2).

Lithium, magnesium and strontium to calcium ratios, in turn, have been suggested as proxies of growth rate or temperature [30–34] (Section 4.2). We did observe considerable similarities between Li/Ca, Mg/Ca, growth rate and temperature (Figures 3–4), but individual samples from a same basket demonstrated variability in element-to-calcium ratios making it difficult to use these ratios as proxies of absolute growth rate or temperature (see Section 4.2). Nevertheless, Li/Ca might reflect crystal growth rate in bivalve shells, whereas Mg/Ca appears to be loosely linked with temperature (Figures 5–6). Finally, individuals within baskets demonstrated variability in Sr/Ca profiles that could not satisfactorily be explained by any single predictor variable (growth rate, temperature, fluorescence and salinity) used in this study (Figure 4).

In general, our results highlight the limitations caused by metabolically controlled deposition of $CaCO_3$ in bivalves [56, 57] suggesting that none of the studied element ratio could be used as straightforward proxies of temperature, salinity, paleoproductivity or shell growth rate. In following sections we discuss the studied element ratios as potential proxies of primary production (Section 4.1), shell growth rate or temperature (Section 4.2), and sub-seasonal temporal anchors (Section 4.3). We also highlight the methodological constraints associated with our data (Section 4.4).

4.1 Potential proxies of primary production

Barium to calcium profiles were characterized by distinct unimodal peaks, which resembled the peaks in fluorescence index (Figures 1, 2, and S1-S6). The barium peak in Kongsfjorden shells occurred approximately 74 days after the peak in phytoplankton bloom, which took place in mid-May, and 19 days after ice-algae/phytoplankton associated fluorescence peak in Rijpfjorden (Table 5). Dissolved barium from seawater, which in turn is sometimes connected with phytoplankton blooms [46, 80], has been found to consistently incorporate into calcitic *Mytilus edulis* and *Pecten maximus* shells with a partition coefficient of approximately 0.1 [39, 49]. Applied to our shells, Ba/Ca values should have been approximately similar, within the averaging error framework (see Section 4.4), in each basket assuming that calcium was uniformly distributed along studied shells. Measured Ba/Ca background values varied between 0.4 and ~ 2

µmol mol^{-1}, were consistent with those reported earlier [46], and did not show any obvious variation within baskets that could not have been explained by averaging error (Table 3). Measured maximum Ba/Ca values, on the other hand, varied between 3.1–76.1 µmol mol^{-1} demonstrating different peak values among shells from a same basket (Table 3). This variability in maximum values is among the largest reported [46], and cannot completely be explained by averaging error (see Section 4.4).

Predictor variables did not satisfactorily explain the Ba/Ca peaks: although Ba/Ca peaks occurred simultaneously with increased shell growth in all growth modeled shells (Figures 2 and S12), growth rate explained only 2% of Ba/Ca variation across samples (marginal R^2 from LMM; Figure 4) and <1 to 18% among samples (R^2 from regression models; Table S2). Further, temperature was negatively related with Ba/Ca explaining 2% of variation across samples (Figure 4). Bivalve age, shell height, or length of the growth increment during mooring deployment did not yield significant slopes in a regression model with Ba/Ca peak values, but Ba/Ca peak values were significantly lower in the 25 m basket in Rijpfjorden compared to other baskets. Therefore, our results are inconclusive about the environmental factors associated with the observed barium peaks. Nevertheless, the considerable differences in Ba/Ca maximums among samples from a same basket and the variable time-lag from bloom between fjords (Table 5) suggest that although Ba/Ca might be connected to processes related to primary production, the ratio cannot be used as a direct paleoproductivity proxy, agreeing with what has been suggested by recent studies [45, 46, 49, 81].

In addition to barium, manganese to calcium profiles also demonstrated peaks that resembled the fluorescence index peaks (Figures 1, 2 and S1-S6). Despite the seemingly synchronous deposition of Mn in growth modeled shells (Table 4), Mn/Ca patterns exhibited individual differences among shells from a same basket (Table 3). Further, Mn/Ca values in the growth modeled shells were clearly correlated with growth rate (Figure 4 and Table S2) demonstrating that Mn/Ca incorporation is likely, at least partly, kinetically controlled. Manganese occurs partly as non-lattice-bound element in an aragonitic bivalve *Corbula amurensis* [82]. A varying amount of Mn not directly bound to $CaCO_3$ matrix could also explain the mixed Mn/Ca results in our study. Nevertheless, Mn/Ca peaks occurring approximately simultaneously in growth modeled shells also demonstrate a degree of synchronous environmental or physiological control. Previous studies suggest that Mn/Ca could partly be incorporated in relationship with Mn concentration in seawater [51, 83]. Phytoplankton blooms have also been suggested as a cause for Mn fluctuations in bivalve shells [24, 38]. Our data do not support the direct connection with phytoplankton bloom events, but it is possible that pelagic Mn cycle is connected to productivity to some extent as reviewed by [83]. Consequently, Mn/Ca is a potential, but complicated proxy of several environmental and physiological factors in both species.

Maximum molybdenum to calcium values were measured during autumn before the deposition of the winter growth band in all growth modeled shells (Figure 2). Consequently, our dataset did not demonstrate prominent Mo peaks occurring during spring as has been reported for calcitic scallops *Comptopallium radula* [48] and *P. maximus* [40]. Nevertheless, Mo/Ca profiles were relatively similar among shells demonstrating that Mo/Ca values either fell under the detection limit of ICP-MS or that the incorporation mechanism could have been environmentally regulated. The incorporation of Mo into bivalve shells might occur through diet, which makes Mo/Ca a promising environmental proxy [40, 49]. If this was the case local phytoplankton may

not have been enriched in Mo. Alternatively, Mo could be connected to sediment surface redox-processes [28] or sediment particles, as bivalves in our study were deployed in the water column and did not grow in their natural habitat. Although our results do not preclude the possibility for Mo/Ca being a potential proxy in *S. groenlandicus* and *C. ciliatum*, more research is needed to draw further conclusions about this elemental ratio.

Our data did not demonstrate a clear connection between fluorescence index and Li/Ca (Figures 4, and S7) casting a doubt on the hypothesis of phytoplankton blooms causing Li/Ca peaks [31]. Therefore, Li/Ca peaks cannot be used as a proxy of timing and magnitude of phytoplankton blooms in studied shells, although it is possible that phytoplankton blooms could have contributed to increasing the Li/Ca values in Kongsfjorden (Table S2).

4.2 Potential proxies of growth rate or temperature

Lithium to calcium patterns were similar among individuals in baskets suggesting synchronized responses to environmental or physiological processes (Figure 2 and Table 3). Logarithm of average growth rate explained 43% of overall Li/Ca variation across all samples (LMM, Figure 4), and 19–75% among samples (regressions, Table S2). Li/Ca–shell growth rate relationships were logarithmic unlike in previous published studies where the authors reported linear relationships with a similar slope for *P. maximus* [31] and *Arctica islandica* [30] (Figure 5A). Shell growth rate is an indicator of crystal growth rate in bivalve mollusk shells [31, 84]. Therefore, the positive correlations between Li/Ca and shell growth rate agree with other published studies suggesting that crystal growth rate is likely the primary driver of Li/Ca incorporation in bivalve mollusk shells [30, 31]. Nevertheless, studies report differing regression equations between Li/Ca and shell growth rate and these relationships do not yield particularly high R^2 values (Figure 5A). This suggests that also other factors affect Li/Ca incorporation.

Temperature and riverine output have also been suggested to partly control Li/Ca in bivalve shells [30, 31]. Since temperature and growth rate were correlated in our shells [17], the effects of these factors are difficult to separate. Nevertheless, temperature significantly explained Li/Ca variability, although these correlations were generally not as strong as for shell growth rate (Figures 4–5 and Table S2). The imprecision in our growth models could have contributed to the lower temperature correlations, as a one-month shift in Li/Ca peak would have led to considerably stronger temperature correlations for Rijpfjorden shells (Figures 2 and S7). Despite this, the relationships for species that have been studied so far do not appear to demonstrate strong enough R^2 values to reconstruct seawater temperatures (Figure 5B). Instead, significant regressions between Li/Ca and temperature in bivalve mollusk shells (Figure 5B) could be explained by dependency between temperature and shell growth rate, and therefore $CaCO_3$ crystal growth rate.

Since we lack element concentration measurements in seawater, we can only speculate about the effect of riverine output increasing Li concentration in ambient water and therefore contributing to shell Li/Ca [30]. Li/Ca peaks were coincident with decreased salinity (Figures 2 and S7). If melt-water events increased Li concentration in ambient water in our study, it is possible that these events could have contributed to Li/Ca fluctuations as suggested by Thébault *et al.* [30]. Despite the uncertainties in our dataset, we can conclude, with a relatively high certainty, that Li/Ca cannot be used as a temperature proxy in *S. groenlandicus* and *C. ciliatum* shells, but

appears to be a promising proxy of shell and/or crystal growth rate. Li/Ca, however, did not yield strong enough relationships to precisely reconstruct sub-annual shell growth.

Relatively consistent patterns in Mg/Ca among individuals from the same basket (Figures 2, S1–S6) suggested that the incorporation of Mg/Ca is likely related to synchronized environmental or physiological processes. A large coefficient of variation, however, indicates that these processes do not yield similar Mg/Ca peak values among shells (Table 3). Relatively strong correlations with logarithm of average growth rate indicated that incorporation of Mg/Ca could be related to shell precipitation rate similarly to Li/Ca (Figure 4). Furthermore, Mg/Ca correlated positively with temperature (Figure 4 and Table S2). Many studies have reported similar significant correlations between Mg/Ca ratio and sea surface temperature [32–35, 44, 53, 85–88]. Most of these studies report either a large variability in temperature correlations similar to our study [e.g. 34, 35], or that the relationship is restricted to certain conditions [e.g. 86, 87]. Organic matter prior the elemental analysis has been removed in some studies that have reported strong relationships between temperature and Mg/Ca [32, 89].

Our Mg/Ca–temperature relationships are similar to those reported for calcitic bivalves *Mytilus trossulus* [32], *M. edulis* [90], and *P. maximus* [88] with the exception that coefficients of variation are clearly lower in our study (Figure 6). Mg/Ca is thought to be strongly metabolically controlled in marine bivalves: present day Mg/Ca molar ratio is 5.2 $\mathrm{mol\,mol^{-1}}$ [91], but report Mg/Ca ratios in bivalve $CaCO_3$ that are several orders of magnitude lower than the ambient molar ratios (varied between 0.0041 and 0.0004 $\mathrm{mol\,mol^{-1}}$ in this study). Furthermore, Mg/Ca is precipitated to inorganic aragonite following an inverse relationship with expected molar ratio of >0.085 $\mathrm{mol\,mol^{-1}}$ for the temperatures in this study [92]. Despite this, most reported Mg/Ca–temperature relationships are positive (Figure 6), *Crassostrea gigas* being an exception [54]. It should also be noted that Mg/Ca–temperature relationships appear generally stronger for calcitic bivalves (bivalves in Figure 6) than for aragonitic bivalves (such as *S. groenlandicus*, *C. ciliatum* and *A. islandica* [e.g. 35]). It seems feasible that Mg/Ca functions as a temperature proxy in many bivalve shells (Figure 6), but Mg/Ca incorporation is also influenced by other factors such that the imprecision associated with temperature estimates derived from Mg/Ca is often larger than the seasonal temperature fluctuations. Our results are consistent with this hypothesis and indicate that Mg/Ca is an unreliable temperature proxy for *S. groenlandicus* and *C. ciliatum*. Nevertheless, our results also indicate that temperature does correlate with Mg incorporation, and further studies should consider removal of organic matter before ICP-MS analyses.

Studies on corals have demonstrated that combining Li/Ca and Mg/Ca could potentially be used to tease apart the metabolic effects associated with these ratios and strengthen the temperature relationship [37]. Our results, however, demonstrated generally weaker correlations between Li/Mg and temperature than those between Li/Ca and temperature and Mg/Ca and temperature separately (Figure 4, Table S2). Consequently, Li/Mg does not provide a robust temperature proxy.

Strontium-to-calcium ratio was significantly affected by all predictor variables (Figure 4), temperature and fluorescence index yielding the most consistent regressions (Table S2). Coefficient of variation for Sr/Ca maximum values indicates that Sr/Ca values varied among samples from a same basket (Table 3). The large variability in Sr/Ca among samples from a same location is consistent with the literature [44, 93] and suggests that any environmental signals

in Sr/Ca may be difficult to separate from vital effects. Strontium partition into calcium carbonate is related to the crystal growth rate of $CaCO_3$ matrix [92, 94]. Although, some earlier studies have successfully used Sr/Ca as a temperature proxy [85, 95, 96], more recent studies question the relationship [50, 97, 98]: it seems possible that temperature and crystal growth rate of $CaCO_3$ skeleton are connected resulting in a positive correlation between Sr/Ca and temperature. Judging from our data, this was not the case for studied shells.

4.3 Sub-seasonal temporal anchors

Barium-to-calcium maximum values were deposited at approximately same time among samples from the same basket (Table 5) considering the uncertainty caused by LA-ICP-MS averaging error and growth models derived from $\delta^{18}O$ values (see Section 4.4). Measured Ba/Ca maximums were estimated to be deposited in mid-July to early August in Kongsfjorden (Table 5). Barium peaks in Rijpfjorden occurred during or right after a fast shell growth period (Figures 2 and S12) and were timed to occur early July in the basket at 15 m depth and late July, 12 days later, in the deeper basket at 25 m depth (Table 5). Simultaneous occurrence of Ba/Ca maximums within baskets and similar patterns in 29 of 32 analyzed shells (Figure S1-S6) indicates synchronous environmental or physiological drivers for incorporation of Ba in studied shells. Synchronously deposited chemical proxies are useful temporal anchors to combine chronologies across bivalves sampled from the same location [29]. Our results indicate that the Ba/Ca peaks are likely to occur simultaneously 2.5 months to 2.5 weeks after primary production bloom, and they can be used as sub-annual anchors across shells from a same location, if averaging error of elemental sampling is kept sufficiently low.

Li/Ca also demonstrated remarkably synchronous patterns within baskets (Table 3) as minimum and maximum value variability could likely be explained by averaging error caused by LA-ICP-MS sampling (see Section 4.4). Therefore, Li/Ca peak and trough values could have been approximately similar across individuals from a same basket further demonstrating the synchronized incorporation of this element ratio. Overall, Li/Ca ratios corresponded with those reported by Thébault *et al.* [30]: the range of Li/Ca fluctuation they reported was 1.3 to 1.6 fold over a growing season, whereas lithium values in this study varied between 1.3 and 2.2 fold (1.6 on average). This demonstrates that Li/Ca could work as a temporal anchor also for other species than *S. groenlandicus* and *C. ciliatum*. Since Li/Ca peaks were rather broad in studied shells it is advisable to use the increases in Li/Ca as temporal anchors.

4.4 Methodological limitations

The bivalves in this study were held in the water column on oceanographic moorings, and therefore they might not have recorded elemental ratios similarly to their natural habitat. The mooring deployment likely excluded the effect of sediment-surface redox-processes, which have been suggested as important contributors for the seasonal dynamics of, at least, Mn [28, 48, 83, 99]. Further, we did not observe similar seasonal patterns in Sr/Ca ratios that has been reported earlier for *S. groenlandicus* [18, 24]. It is possible that Sr/Ca is partly connected with sediment surface processes and therefore our shells did not record all possible variability for this element ratio.

The extent of time averaging sampled by LA-ICP-MS is relative to the sample volume and average shell growth rate over the sampled area [71, 72]. Because sample hole size in our study varied little within years (see Section 2.2), time averaging was related to shell growth rate. Even though LA-ICP-MS sampling was able to capture the Ba/Ca peaks (Figures 2, S1–S6) it is possible that time-averaging contributed to profiles of some elements during low growth rate such that no meaningful environmental correlations were found [100].

Growth models used to determine the time extent for each LA-ICP-MS sample were subject to uncertainty [17]. It is unlikely that these growth models were an entirely accurate representation of the actual growth during the mooring deployment and, therefore, our dataset contained a bias, which increased correlations between element ratios and average shell growth rate, because shell growth rate was obtained from growth models, which affected the alignment of elemental ratios. Further, shell growth rate and temperature were significantly correlated in all growth modeled shells (Figure 3; 17).

Even though we attempted to keep LA-ICP-MS samples as close to the middle of the shell section as possible, non-linear growth patterns could have caused variations in the actual location of LA-ICP-MS samples hence affecting the element ratios [101], since the sample spot alignment method used in this study [69] could not correct for measurement bias caused by variability in $CaCO_3$ matrix. Furthermore, the sample alignment method assumed two-dimensional sampling ignoring any effects of LA-ICP-MS sample volume. Consequently, the curvature of growth lines deeper in the sample could have increased imprecision of element ratios through three-dimensional time averaging. Despite all these uncertainties, our dataset is extensive and clearly indicates that all of the studied elemental ratios were affected by several factors to the extent that no element ratio in this study could be used as an absolute straightforward proxy of temperature, salinity, fluorescence or shell growth rate.

5 Conclusions

We conclude that Ba/Ca, Li/Ca and Mg/Ca have a potential as environmental proxies in *S. groenlandicus* and *C. ciliatum* shells: Incorporation of Ba/Ca might be connected with seasonal dissolved or particular Ba dynamics in ambient water, and incorporation of Li/Ca and Mg/Ca are likely connected with both $CaCO_3$ crystal growth rate and seawater temperature. Despite this, all studied element ratios were likely affected by multiple internal and external factors complicating the interpretation of element ratios. Our study was further affected by methodological constraints, such as time-averaging error, experimental artifacts, and uncertainties in sub-annual growth models leading to partly inconclusive results for Sr/Ca and Mo/Ca. Despite this our results are an important contribution to high-latitude bivalve shell geochemisty highlighting that none of the studied elemental ratios can be used as all-encompassing proxies of seawater temperature, salinity, paleoproductivity, or shell growth rate. This, however, does not preclude the use of element-to-calcium ratios as environmental proxies, but merely indicates that seasonal dynamics of elements in seawater and seasonal variations in bivalve metabolism must be understood better to link the elemental ratios in bivalve mollusk shells with environmental processes.

Acknowledgments

We acknowledge the use of the NSF-supported WHOI ICP-MS facility and thank Scot Birdwhistell for his excellent assistance. We are grateful to Bates Imaging Center and William Ash for help with thick-section photographs. Further, we want to thank the Stack Exchange community for help with the graphical presentation and data-analysis, and the R community for maintaining open source statistics tools used in this study. This research was financed through the UiT The Arctic University of Norway Utenlandstipend (MV), the EU 7th Framework Program project Arctic Tipping Points (contract number FP7-ENV-2009-226248; http://www.eu-atp.org; PER), the Research Council of Norway project Havet og Kysten (184719/S40; PER), the Norwegian Polar Institute (HH, MV) and Akvaplan-niva (PER, MV, WGA, MLC).

References

1. Vaughan, D.; Comiso, J.; Allison, I.; Carrasco, J.; Kaser, G.; Kwok, R.; Mote, P.; Murray, T.; Paul, F.; Ren, J.; Rignot, E.; Solomina, O.; Steffen, K.; Zhang, T. Observations: Cryosphere. In *Climate Change 2013: The Physical Science Basis Contribution of Working Group I to the Fifth Assessment Report of the Intergovernmental Panel on Climate Change*; Stocker, T.; Qin, D.; Plattner, G.K.; Tignor, M.; Allen, S.; Boschung, J.; Nauels, A.; Xia, Y.; Bex, V.; Midgley, P., Eds.; Cambridge University Press: Cambridge, UK and New York, NY, USA, 2013; chapter 4, pp. 317–382.

2. AMAP. Arctic climate issues 2011: Changes in Arctic snow, water, ice and permafrost. SWIPA 2011 Overview report. Technical report, Arctic Monitoring and Assessment Programme (AMAP), Oslo, Norway, 2012.

3. Grebmeier, J.M. Shifting patterns of life in the Pacific Arctic and sub-Arctic seas. *Ann Rev Mar Sci* **2012**, *4*, 63–78.

4. Masson-Delmotte, V.; Schulz, M.; Abe-Ouchi, A.; Beer, J.; Ganopolski, A.; Rouco, J.G.; Jansen, E.; Lambeck, K.; Luterbacher, J.; Naish, T.; Osborn, T.; Otto-Bliesner, B.; Quinn, T.; Ramesh, R.; Rojas, M.; Shao, X.; Timmermann, A. Information from paleoclimate archives. In *Climate Change 2013: The Physical Science Basis Contribution of Working Group I to the Fifth Assessment Report of the Intergovernmental Panel on Climate Change*; Stocker, T.; Qin, D.; Plattner, G.K.; Tignor, M.; Allen, S.; Boschung, J.; Nauels, A.; Xia, Y.; Bex, V.; Midgley, P., Eds.; Cambridge University Press: Cambridge, UK and New York, NY, USA, 2013; chapter 5, pp. 383–464.

5. Pearson, P.N.; Palmer, M.R. Atmospheric carbon dioxide concentrations over the past 60 million years. *Nature* **2000**, *406*, 695–699.

6. Zachos, J.; Pagani, M.; Sloan, L.; Thomas, E.; Billups, K. Trends, rhythms, and aberrations in global climate 65 Ma to present. *Science* **2001**, *292*, 686–93.

7. Dame, R.F. Introduction. In *Ecology of Marine Bivalves, An Ecosystem Approach*; CRC Press: Boca Raton, FL, USA, 2012; pp. 1–19.

8. Krantz, D.E.; Williams, D.F.; Jones, D.S. Ecological and paleoenvironmental information using stable isotope profiles from living and fossil molluscs. *Palaeogeogr Palaeoclimatol Palaeoecol* **1987**, *58*, 249–266.

9. Valentine, J.W.; Jablonski, D.; Kidwell, S.; Roy, K. Assessing the fidelity of the fossil record by using marine bivalves. *Proc Natl Acad Sci U S A* **2006**, *103*, 6599–6604.

10. Clapham, M.E.; Bottjer, D.J. Permian marine paleoecology and its implications for large-scale decoupling of brachiopod and bivalve abundance and diversity during the Lopingian (Late Permian). *Palaeogeogr Palaeoclimatol Palaeoecol* **2007**, *249*, 283–301.

11. Strom, A.; Francis, R.C.; Mantua, N.J.; Miles, E.L.; Peterson, D.L. North Pacific climate recorded in growth rings of geoduck clams: A new tool for paleoenvironmental reconstruction. *Geophys Res Lett* **2004**, *31*, L06206.

12. Wanamaker, A.D.; Butler, P.G.; Scourse, J.D.; Heinemeier, J.; Eiríksson, J.; Knudsen, K.L.; Richardson, C.A. Surface changes in the North Atlantic meridional overturning circulation during the last millennium. *Nat Commun* **2012**, *3*, 1–7.

13. Butler, P.G.; Wanamaker, A.D.; Scourse, J.D.; Richardson, C.A.; Reynolds, D.J. Variability of marine climate on the North Icelandic Shelf in a 1357-year proxy archive based on growth increments in the bivalve *Arctica islandica*. *Palaeogeogr Palaeoclimatol Palaeoecol* **2013**, *373*, 141–151.

14. Chauvaud, L.; Thouzeau, G.; Paulet, Y.M. Effects of environmental factors on the daily growth rate of *Pecten maximus* juveniles in the Bay of Brest (France). *J Exp Mar Bio Ecol* **1998**, *227*, 83–111.

15. Schöne, B.R.; Houk, S.D.; Castro, A.D.F.; Fiebig, J.; Oschmann, W.; Kroncke, I.; Dreyer, W.; Gosselck, F. Daily growth rates in shells of *Arctica islandica*: Assessing sub-seasonal environmental controls on a long-lived bivalve mollusk. *Palaios* **2005**, *20*, 78–92.

16. Chauvaud, L. Shell of the Great Scallop Pecten maximus as a high-frequency archive of paleoenvironmental changes. *Geochemistry Geophys Geosystems* **2005**, *6*, 1–15.

17. Vihtakari, M.; Renaud, P.E.; Clarke, L.J.; Whitehouse, M.J.; Hop, H.; Carroll, M.L.; Ambrose Jr, W.G. Decoding the oxygen isotope signal for seasonal growth patterns in Arctic bivalves. *In prep.* **2014**.

18. Ambrose Jr, W.G.; Carroll, M.L.; Greenacre, M.J.; Thorrold, S.R.; McMahon, K.W. Variation in *Serripes groenlandicus* (Bivalvia) growth in a Norwegian high-Arctic fjord: evidence for local- and large-scale climatic forcing. *Glob Chang Biol* **2006**, *12*, 1595–1607.

19. Sejr, M.K.; Blicher, M.E.; Rysgaard, S. Sea ice cover affects inter-annual and geographic variation in growth of the Arctic cockle *Clinocardium ciliatum* (Bivalvia) in Greenland. *Mar Ecol Ser* **2009**, *389*, 149–158.

20. Carroll, M.L.; Ambrose Jr, W.G.; Levin, B.S.; Ryan, S.K.; Ratner, A.R.; Henkes, G.A.; Greenacre, M.J. Climatic regulation of *Clinocardium ciliatum* (Bivalvia) growth in the northwestern Barents Sea. *Palaeogeogr Palaeoclimatol Palaeoecol* **2011**, *302*, 10–20.

21. Carroll, M.L.; Ambrose Jr, W.G.; Levin, B.S.; Locke V, W.L.; Henkes, G.A.; Hop, H.; Renaud, P.E. Pan-Svalbard growth rate variability and environmental regulation in the Arctic bivalve *Serripes groenlandicus*. *J Mar Syst* **2011**, *88*, 239–251.

22. Carroll, M.L.; Ambrose Jr, W.G.; Locke V, W.L.; Ryan, S.K.; Johnson, B.J.; Jr, W.G.A.; V, W.L.L. Bivalve growth rate and isotopic variability across the Barents Sea Polar Front. *J Mar Syst* **2014**, *130*, 167–180.

23. Khim, B.K.; Krantz, D.E.; Cooper, L.W.; Grebmeier, J.M. Seasonal discharge of estuarine freshwater to the western Chukchi Sea shelf identified in stable isotope profiles of mollusk shells. *J Geophys Res* **2003**, *108*, 1–10.

24. Carroll, M.L.; Johnson, B.J.; Henkes, G.A.; McMahon, K.W.; Voronkov, A.; Ambrose Jr, W.G.; Denisenko, S.G. Bivalves as indicators of environmental variation and potential anthropogenic impacts in the southern Barents Sea. *Mar Pollut Bull* **2009**, *59*, 193–206.

25. Henkes, G.A.; Passey, B.H.; Wanamaker, A.D.; Grossman, E.L.; Ambrose Jr, W.G.; Carroll, M.L. Carbonate clumped isotope compositions of modern marine mollusk and brachiopod shells. *Geochim Cosmochim Acta* **2013**, *106*, 307–325.

26. Ambrose Jr, W.G.; Renaud, P.E.; Locke V, W.L.; Cottier, F.R.; Berge, J.; Carroll, M.L.; Levin, B.; Ryan, S. Growth line deposition and variability in growth of two circumpolar bivalves (*Serripes groenlandicus*, and *Clinocardium ciliatum*). *Polar Biol* **2012**, *35*, 345–354.

27. Henderson, G.M. New oceanic proxies for paleoclimate. *Earth Planet Sci Lett* **2002**, *203*, 1–13.

28. Tribovillard, N.; Algeo, T.J.; Lyons, T.; Riboulleau, A. Trace metals as paleoredox and paleoproductivity proxies: An update. *Chem Geol* **2006**, *232*, 12–32.

29. Wanamaker, A.D.; Hetzinger, S.; Halfar, J. Reconstructing mid- to high-latitude marine climate and ocean variability using bivalves, coralline algae, and marine sediment cores from the Northern Hemisphere. *Palaeogeogr Palaeoclimatol Palaeoecol* **2011**, *302*, 1–9.

30. Thébault, J.; Schöne, B.R.; Hallmann, N.; Barth, M.; Nunn, E.V. Investigation of Li/Ca variations in aragonitic shells of the ocean quahog *Arctica islandica*, northeast Iceland. *Geochemistry Geophys Geosystems* **2009**, *10*, 1–15.

31. Thébault, J.; Chauvaud, L. Li/Ca enrichments in great scallop shells (*Pecten maximus*) and their relationship with phytoplankton blooms. *Palaeogeogr Palaeoclimatol Palaeoecol* **2013**, *373*, 108–122.

32. Klein, R.T.; Lohmann, K.C.; Thayer, C.W. Bivalve skeletons record sea-surface temperature and $\delta^{18}O$ via Mg/Ca and $^{18}O/^{16}O$ ratios. *Geology* **1996**, *24*, 415–418.

33. Pearce, N.J.G.; Mann, V.L. Trace metal variations in the shells of *Ensis siliqua* record pollution and environmental conditions in the sea to the west of mainland Britain. *Mar Pollut Bull* **2006**, *52*, 739–55.

34. Richardson, C. Age, growth rate and season of recruitment of *Pinna nobilis* (L) in the Croatian Adriatic determined from Mg:Ca and Sr:Ca shell profiles. *J Exp Mar Bio Ecol* **2004**, *299*, 1–16.

35. Schöne, B.R.; Zhang, Z.J.; Radermacher, P.; Thebault, J.; Jacob, D.E.; Nunn, E.V.; Maurer, A.F. Sr/Ca and Mg/Ca ratios of ontogenetically old, long-lived bivalve shells (*Arctica islandica*) and their function as paleotemperature proxies. *Palaeogeogr Palaeoclimatol Palaeoecol* **2011**, *302*, 52–64.

36. Vihtakari, M. Bivalves as indicators of environmental perturbations related to climate and ocean acidification. Phd thesis, UiT The Arctic University of Norway, 2014.

37. Robinson, L.F.; Adkins, J.F.; Frank, N.; Gagnon, A.C.; Prouty, N.G.; Brendan Roark, E.; de Flierdt, T.V. The geochemistry of deep-sea coral skeletons: A review of vital effects and applications for palaeoceanography. *Deep Sea Res Part 2 Top Stud Oceanogr* **2014**, *99*, 184–198.

38. Vander Putten, E.; Dehairs, F.; Keppens, E. High resolution distribution of trace elements in the calcite shell layer of modern *Mytilus edulis*: Environmental and biological controls. *Geochim Cosmochim Acta* **2000**, *64*, 997–1011.

39. Gillikin, D.; Dehairs, F.; Lorrain, A.; Steenmans, D.; Baeyens, W.; Andre, L. Barium uptake into the shells of the common mussel (*Mytilus edulis*) and the potential for estuarine paleo-chemistry reconstruction. *Geochim Cosmochim Acta* **2006**, *70*, 395–407.

40. Barats, A.; Amouroux, D.; Chauvaud, L. Spring molybdenum enrichment in scallop shells: a potential tracer of diatom productivity in temperate coastal environments (Brittany, NW France). *Biogeosciences* **2010**, *7*, 233–245.

41. Stecher, H.A.I.; Krantz, D.E.; Lord, C.J.I.; Luther, G.W.I.; Bock, K.W. Profiles of strontium and barium in *Mercenaria mercenaria* and *Spisula solidissima* shells. *Geochim Cosmochim Acta* **1996**, *60*, 3445–3456.

42. Toland, H.; Perkins, B.; Pearce, N.J.G.; Keenan, F.; Leng, M.J. A study of sclerochronology by laser ablation ICP-MS. *J Anal At Spectrom* **2000**, *15*, 1143–1148.

43. Torres, M.; Barry, J.; Hubbard, D. Reconstructing the history of fluid flow at cold seep sites from Ba/Ca ratios in vesicomyid clam shells. *Limnol Oceanogr* **2001**, *46*, 1701–1708.

44. Lazareth, C.; Putten, E.; André, L.; Dehairs, F. High-resolution trace element profiles in shells of the mangrove bivalve *Isognomon ephippium*: a record of environmental spatio-temporal variations? *Estuar Coast Shelf Sci* **2003**, *57*, 1103–1114.

45. Gillikin, D.P.; Lorrain, A.; Paulet, Y.m.; André, L.; Dehairs, F. Synchronous barium peaks in high-resolution profiles of calcite and aragonite marine bivalve shells. *Geo-Marine Lett* **2008**, *28*, 351–358.

46. Barats, A.; Amouroux, D.; Chauvaud, L.; Pécheyran, C.; Lorrain, A.; Thébault, J.; Church, T.M.; Donard, O.F.X. High frequency Barium profiles in shells of the Great Scallop *Pecten maximus*: a methodical long-term and multi-site survey in Western Europe. *Biogeosciences* **2009**, *6*, 157–170.

47. Elliot, M.; Welsh, K.; Chilcott, C.; McCulloch, M.; Chappell, J.; Ayling, B. Profiles of trace elements and stable isotopes derived from giant long-lived *Tridacna gigas* bivalves: Potential applications in paleoclimate studies. *Palaeogeogr Palaeoclimatol Palaeoecol* **2009**, *280*, 132–142.

48. Thébault, J.; Chauvaud, L.; L'Helguen, S.; Clavier, J.; Barats, A.; Jacquet, S.; Pecheyran, C.; Amouroux, D. Barium and molybdenum records in bivalve shells: Geochemical proxies for phytoplankton dynamics in coastal environments? *Limnol Oceanogr* **2009**, *54*, 1002–1014.

49. Tabouret, H.; Pomerleau, S.; Jolivet, A.; Pécheyran, C.; Riso, R.; Thébault, J.; Chauvaud, L.; Amouroux, D. Specific pathways for the incorporation of dissolved barium and molybdenum into the bivalve shell: an isotopic tracer approach in the juvenile Great Scallop (*Pecten maximus*). *Mar Environ Res* **2012**, *78*, 15–25.

50. Carre, M.; Bentaleb, I.; Bruguier, O.; Ordinola, E.; Barrett, N.; Fontugne, M. Calcification rate influence on trace element concentrations in aragonitic bivalve shells: Evidences and mechanisms. *Geochim Cosmochim Acta* **2006**, *70*, 4906–4920.

51. Freitas, P.S.; Clarke, L.J.; Kennedy, H.; Richardson, C.A.; Abrantes, F. Environmental and biological controls on elemental (Mg/Ca, Sr/Ca and Mn/Ca) ratios in shells of the king scallop *Pecten maximus*. *Geochim Cosmochim Acta* **2006**, *70*, 5119–5133.

52. Shirai, K.; Takahata, N.; Yamamoto, H.; Omata, T.; Sasaki, T.; Sano, Y. Novel analytical approach to bivalve shell biogeochemistry: A case study of hydrothermal mussel shell. *Geochem J* **2008**, *42*, 413–420.

53. Freitas, P.S.; Clarke, L.J.; Kennedy, H.A.; Richardson, C.A. Ion microprobe assessment of the heterogeneity of Mg/Ca, Sr/Ca and Mn/Ca ratios in *Pecten maximus* and *Mytilus edulis* (Bivalvia) shell calcite precipitated at constant temperature. *Biogeosciences* **2009**, *6*, 1209–1227.

54. Ullmann, C.V.; Böhm, F.; Rickaby, R.E.; Wiechert, U.; Korte, C. The Giant Pacific Oyster (*Crassostrea gigas*) as a modern analog for fossil ostreoids: Isotopic (Ca, O, C)

and elemental (Mg/Ca, Sr/Ca, Mn/Ca) proxies. *Geochemistry, Geophys Geosystems* **2013**, *14*, 4109–4120.

55. Wassmann, P.; Duarte, C.M.; Agustí, S.; Sejr, M.K. Footprints of climate change in the Arctic marine ecosystem. *Glob Chang Biol* **2011**, *17*, 1235–1249.

56. Checa, A. A new model for periostracum and shell formation in Unionidae (Bivalvia, Mollusca). *Tissue & Cell* **2000**, *32*, 405–416.

57. Schöne, B.R. The curse of physiology - challenges and opportunities in the interpretation of geochemical data from mollusk shells. *Geo-Marine Lett* **2008**, *28*, 269–285.

58. Marin, F. The formation and mineralization of mollusk shell. *Front Biosci* **2012**, *S4*, 1099–1125.

59. Svendsen, H.; Beszczynska-Møller, A.; Hagen, J.O.; Lefauconnier, B.; Tverberg, V.; Gerland, S.; Ø rbæk, J.B.; Bischof, K.; Papucci, C.; Zajaczkowski, M.; Azzolini, R.; Bruland, O.; Wiencke, C.; Winther, J.G.; Dallmann, W. The physical environment of Kongsfjorden – Krossfjorden, an Arctic fjord system in Svalbard. *Polar Res* **2002**, *21*, 133–166.

60. Howe, J.A.; Harland, R.; Cottier, F.R.; Brand, T.; Willis, K.J.; Berge, J.r.R.; Grosfjeld, K.; Eriksson, A. Dinoflagellate cysts as proxies for palaeoceanographic conditions in Arctic fjords. *Geol Soc Spec Publ* **2010**, *344*, 61–74.

61. Wallace, M.I.; Cottier, F.R.; Berge, J.; Tarling, G.A.; Griffiths, C.; Brierley, A.S. Comparison of zooplankton vertical migration in an ice-free and a seasonally ice-covered Arctic fjord: An insight into the influence of sea ice cover on zooplankton behavior. *Limnol Oceanogr* **2010**, *55*, 831–845.

62. Søreide, J.E.; Leu, E.; Berge, J.; Graeve, M.; Falk-Petersen, S. Timing of blooms, algal food quality and *Calanus glacialis* reproduction and growth in a changing Arctic. *Glob Chang Biol* **2010**, *16*, 3154–3163.

63. Norwegian Meteorological Institute. Icechart archive. Polar View – European Arctic node, 2014. `http://polarview.met.no`, accessed on 2014-04-01.

64. Mokgalaka, N.S.; Gardea-Torresdey, J.L. Laser ablation inductively coupled plasma mass spectrometry: principles and applications. *Appl Spectrosc Rev* **2006**, *41*, 131–150.

65. Vander Putten, E.; Dehairs, F.; André, L.; Baeyens, W. Quantitative in situ microanalysis of minor and trace elements in biogenic calcite using infrared laser ablation inductively coupled plasma mass spectrometry: a critical evaluation. *Anal Chim Acta* **1999**, *378*, 261–272.

66. Yoshinaga, J.; Nakama, A.; Morita, M.; Edmonds, J.S. Fish otolith reference material for quality assurance of chemical analyses. *Mar Chem* **2000**, *69*, 91–97.

67. Sturgeon, R.E.; Willie, S.N.; Yang, L.; Greenberg, R.; Spatz, R.O.; Chen, Z.; Scriver, C.; Clancy, V.; Lam, J.W.; Thorrold, S. Certification of a fish otolith reference material in support of quality assurance for trace element analysis. *J Anal At Spectrom* **2005**, *20*, 1067–1071.

68. Schneider, C.A.; Rasband, W.S.; Eliceiri, K.W. NIH Image to ImageJ: 25 years of image analysis. *Nat Methods* **2012**, *9*, 671–675.

69. Vihtakari, M. sclero: measure growth patterns and align sampling spots in photographs. R package version 0.1, 2014. `https://github.com/MikkoVihtakari/sclero`.

70. R Core Team. R: A language and environment for statistical computing. R Foundation for Statistical Computing, Vienna, Austria, 2014. `http://www.r-project.org`.

71. Goodwin, D.; Flessa, K.; Tellezduarte, M.; Dettman, D.; Schöne, B.R.; Avilaserrano, G. Detecting time-averaging and spatial mixing using oxygen isotope variation: a case study. *Palaeogeogr Palaeoclimatol Palaeoecol* **2004**, *205*, 1–21.

72. Beelaerts, V.; Ridder, F.; Schmitz, N.; Bauwens, M.; Dehairs, F.; Schoukens, J.; Pintelon, R. On the elimination of bias averaging-errors in proxy records. *Math Geosci* **2008**, *41*, 129–144.

73. Barton, K. MuMIn: Multi-model inference. R package version 1.10.5., 2014. `http://cran.r-project.org/package=MuMIn`.

74. Johnson, P.C. Extension of Nakagawa & Schielzeth's R^2_{GLMM} to random slopes models. *Methods Ecol Evol* **2014**, *5*, 944–946.

75. Pinheiro, J.; Bates, D. nlme: Linear and Nonlinear Mixed Effects Models, 2014. `http://cran.r-project.org/package=nlme`.

76. Pearson, K. On lines and planes of closest fit to systems of points in space. *Philos Mag* **1901**, *2*, 559–572.

77. Fisher, R.A. On the "Probable Error" of a Coefficient of Correlation deduced from a Small Sample. *Metron* **1921**, *1*, 3–32.

78. Corey, D.M.; Dunlap, W.P.; Burke, M.J. Averaging Correlations: Expected Values and Bias in Combined Pearson r s and Fisher's z Transformations. *J Gen Psychol* **1998**, *125*, 245–261.

79. Bonett, D.G.; Wright, T.A. Sample size requirements for estimating Pearson, Kendall and Spearman correlations. *Psychometrika* **2000**, *65*, 23–28.

80. Fisher, N.S.; Guillard, R.R.L.; Bankston, D.C. The accumulation of barium by marine phytoplankton grown in culture. *J Mar Res* **1991**, *49*, 339–354.

81. Goodwin, D.H.; Gillikin, D.P.; Roopnarine, P.D. Preliminary evaluation of potential stable isotope and trace element productivity proxies in the oyster *Crassostrea gigas*. *Palaeogeogr Palaeoclimatol Palaeoecol* **2013**, *373*, 88–97.

82. Takesue, R.; Bacon, C.; Thompson, J. Influences of organic matter and calcification rate on trace elements in aragonitic estuarine bivalve shells. *Geochim Cosmochim Acta* **2008**, *72*, 5431–5445.

83. Barats, A.; Amouroux, D.; Pécheyran, C.; Chauvaud, L.; Donard, O.F.X. High-frequency archives of manganese inputs to coastal waters (Bay of Seine, France) resolved by the LA-ICP-MS analysis of calcitic growth layers along scallop shells (*Pecten maximus*). *Environ Sci Technol* **2008**, *42*, 86–92.

84. Lorrain, A.; Paulet, Y.M.; Chauvaud, L.; Dunbar, R.; Mucciarone, D.; Fontugne, M. δ^{13}C variation in scallop shells: Increasing metabolic carbon contribution with body size? *Geochim Cosmochim Acta* **2004**, *68*, 3509–3519.

85. Dodd, J. Environmental control of strontium and magnesium in *Mytilus*. *Geochim Cosmochim Acta* **1965**, *29*, 385–398.

86. Freitas, P.; Clarke, L.J.; Kennedy, H.; Richardson, C.A.; Abrantes, F. Mg/Ca, Sr/Ca, and stable-isotope (δ^{18}O and δ^{13}C) ratio profiles from the fan mussel *Pinna nobilis*: Seasonal records and temperature relationships. *Geochemistry Geophys Geosystems* **2005**, *6*, 1–16.

87. Wanamaker, A.D.; Kreutz, K.J.; Wilson, T.; Borns Jr, H.W.; Introne, D.S.; Feindel, S. Experimentally determined Mg/Ca and Sr/Ca ratios in juvenile bivalve calcite for *Mytilus edulis*: implications for paleotemperature reconstructions. *Geo-Marine Lett* **2008**, *28*, 359–368.

88. Freitas, P.S.; Clarke, L.J.; Kennedy, H.; Richardson, C.A. The potential of combined Mg/Ca and δ^{18}O measurements within the shell of the bivalve *Pecten maximus* to estimate seawater δ^{18}O composition. *Chem Geol* **2012**, *291*, 286–293.

89. Klein, R.T.; Lohmann, K.C.; Kennedy, G.L. Elemental and isotopic proxies of paleotemperature and paleosalinity: Climate reconstruction of the marginal northeast Pacific ca. 80 ka. *Geology* **1997**, *25*, 363.

90. Freitas, P.S.; Clarke, L.J.; Kennedy, H.A.; Richardson, C.A. Inter- and intra-specimen variability masks reliable temperature control on shell Mg/Ca ratios in laboratory and field cultured *Mytilus edulis* and *Pecten maximus* (Bivalvia). *Biogeosciences* **2008**, *5*, 1245–1258.

91. Stanley, S.M.; Hardie, L.A. Secular oscillations in the carbonate mineralogy of reef-building and sediment-producing organisms driven by tectonically forced shifts in seawater chemistry. *Palaeogeogr Palaeoclimatol Palaeoecol* **1998**, *144*, 3–19.

92. Gaetani, G.A.; Cohen, A.L. Element partitioning during precipitation of aragonite from seawater: A framework for understanding paleoproxies. *Geochim Cosmochim Acta* **2006**, *70*, 4617–4634.

93. Gillikin, D.P.; Lorrain, A.; Navez, J.; Taylor, J.W.; André, L.; Keppens, E.; Baeyens, W.; Dehairs, F. Strong biological controls on Sr/Ca ratios in aragonitic marine bivalve shells. *Geochemistry Geophys Geosystems* **2005**, *6*, 1–16.

94. Carpenter, S.J.; Lohmann, K.C. Sr/Mg ratios of modern marine calcite: Empirical indicators of ocean chemistry and precipitation rate. *Geochim Cosmochim Acta* **1992**, *56*, 1837–1849.

95. Beck, J.W.; Edwards, R.L.; Ito, E.; Taylor, F.W.; Recy, J.; Rougerie, F.; Joannot, P.; Henin, C. Sea-surface temperature from coral skeletal strontium/calcium ratios. *Science* **1992**, *257*, 644–647.

96. Alibert, C.; McCulloch, M.T. Strontium/calcium ratios in modern *Porites* corals from the Great Barrier Reef as a proxy for sea surface temperature: Calibration of the thermometer and monitoring of ENSO. *Paleoceanography* **1997**, *12*, 345–363.

97. Saenger, C.; Cohen, A.L.; Oppo, D.W.; Hubbard, D. Interpreting sea surface temperature from strontium/calcium ratios in *Montastrea* corals: Link with growth rate and implications for proxy reconstructions. *Paleoceanography* **2008**, *23*, PA3102:1–11.

98. Schöne, B.R.; Radermacher, P.; Zhang, Z.; Jacob, D.E. Crystal fabrics and element impurities (Sr/Ca, Mg/Ca, and Ba/Ca) in shells of *Arctica islandica* - Implications for paleoclimate reconstructions. *Palaeogeogr Palaeoclimatol Palaeoecol* **2013**, *373*, 50–59.

99. Dehairs, F.; Baeyens, W.; Van Gansbeke, D. Tight coupling between enrichment of iron and manganese in North Sea suspended matter and sedimentary redox processes: Evidence for seasonal variability. *Estuar Coast Shelf Sci* **1989**, *29*, 457–471.

100. Shirai, K.; Schöne, B.R.; Miyaji, T.; Radarmacher, P.; Krause, R.a.; Tanabe, K. Assessment of the mechanism of elemental incorporation into bivalve shells (*Arctica islandica*) based on elemental distribution at the microstructural scale. *Geochim Cosmochim Acta* **2014**, *126*, 307–320.

101. Lazareth, C.; Le Cornec, F.; Candaudap, F.; Freydier, R. Trace element heterogeneity along isochronous growth layers in bivalve shell: Consequences for environmental reconstruction. *Palaeogeogr Palaeoclimatol Palaeoecol* **2013**, *373*, 39–49.

Tables

Table 1. Total number of LA-ICP-MS analyzed bivalve specimens. Numbers in parentheses indicate the number of samples with growth models determined through SIMS $\delta^{18}O$ measurements. Basket abbreviations used through out this study are specified in "Basket" column.

Year	Fjord	Depth (m)	Basket	*Serripes*	*Ciliatocardium*
2007-2008	Kongsfjorden	25	KB	2	2
2007-2008	Rijpfjorden	25	RB	2	2
2009-2010	Kongsfjorden	15	RA	2	3
2009-2010	Rijpfjorden	15	RA	3 (2)	1 (1)
2009-2010	Kongsfjorden	25	RB	4 (2)	1 (1)
2009-2010	Rijpfjorden	25	RB	4 (2)	4 (1)

Table 2. Depths (m) of mooring instruments used to record environmental variables.

		2007-2008		2009-2010	
Variable	Instrument	Kongsfjorden	Rijpfjorden	Kongsfjorden	Rijpfjorden
Temperature	TidBit	15 & 25		15 & 25	
Fluorescence	Fluorometer	30	17	36	10
Salinity	CTD	30	17	36	10 & 26

Table 3. Mean values ($\bar{x}$) and coefficient of variation (CV) of maximum and minimum element ratios measured along shell sections. Year 2010 refers to the deployment period 2009-2010 and year 2008 to the deployment period 2007-2008. Number of samples is specified in "n" column. See Table 1 for basket abbreviations.

				Minimum		Maximum	
Ratio	Year	Basket	n	$\bar{x}$	CV	$\bar{x}$	CV
Li/Ca	2010	KA	5	13.6	14.1	22.5	4.4
	2010	KB	5	13.1	13.5	21.9	6.0
	2010	RA	4	14.9	7.5	22.0	1.8
	2010	RB	8	14.1	9.0	20.8	6.9
Mg/Ca	2008	KB	4	0.90	30.4	2.40	37.5
	2008	RB	4	0.63	34.4	1.87	39.2
	2010	KA	5	1.11	35.0	3.04	9.0
	2010	KB	5	0.87	31.3	3.13	6.3
	2010	RA	4	1.28	6.7	3.14	21.6
	2010	RB	8	1.22	25.1	2.90	29.1
Li/Mg	2010	KA	5	6.7	10.4	13.9	34.5
	2010	KB	5	6.2	13.7	18.2	13.8
	2010	RA	4	6.7	20.2	13.3	8.6
	2010	RB	8	6.9	25.3	12.9	21.0
Mn/Ca	2008	KB	4	0.38	56.0	8.52	107.8
	2008	RB	4	0.75	77.9	7.52	84.2
	2010	KA	5	0.19	45.6	3.75	32.9
	2010	KB	5	0.16	41.8	1.31	51.8
	2010	RA	4	0.17	25.0	1.89	48.8
	2010	RB	8	0.20	65.8	1.68	51.2
Sr/Ca	2008	KB	4	1.23	8.8	2.53	21.9
	2008	RB	4	1.36	22.1	2.63	35.4
	2010	KA	5	1.35	13.7	2.32	17.5
	2010	KB	5	1.28	6.2	2.17	10.0
	2010	RA	4	1.47	24.8	2.53	13.7
	2010	RB	8	1.28	7.3	2.24	18.0
Ba/Ca	2008	KB	4	0.61	10.8	49.1	23.6
	2008	RB	4	0.74	25.5	25.2	139.9
	2010	KA	5	0.69	18.2	11.2	48.2
	2010	KB	5	0.50	10.9	14.0	47.8
	2010	RA	4	0.67	30.8	17.1	25.1
	2010	RB	8	0.52	11.0	4.3	27.2

Table 4. Manganese to calcium peaks and their relation to spring bloom peaks determined from fluorescence index for samples with growth models. Columns from the left: Sample = sample IDs and basket averages corresponding to Vihtakari *et al.* [17]; Treatment = treatment basket, see Table 1; Species: Ser = *S. groenlandicus*, and Cil = *C. ciliatum*; Mn/Ca max = maximum measured Mn/Ca ratio; Timing of Mn/Ca max = estimated timing for the Mn/Ca peak using centroids, and minimum (Min) and maximum (Max) extent of a LA-ICP-MS hole. Minimum (Min) and maximum (Max) are expressed as days from the centroid; After fluorescence peak = indicating how many days after the spring bloom peak when the Mn/Ca maximum took place.

				Timing of Mn/Ca max			After fluorescence peak		
Sample	Basket	Species	Mn max ($\mu mol\,mol^{-1}$)	Centroid (date)	Min (-days)	Max (+days)	Centroid (days)	Min (days)	Max (days)
A	KB	Ser	1.4	19 Jul	4	5	65	61	70
B	KB	Ser	1.0	28 May	12	55	13	1	68
C	KB	Cil	0.6	1 Jun	3	33	17	14	50
Average	KB		1.0	15 Jun	6	31	32	25	63
D	RA	Ser	2.9	5 Jul	1	8	12	11	20
E	RA	Ser	1.2	5 Jul	2	5	12	10	17
F	RA	Cil	0.9	22 Jul	0	1	29	29	30
Average	RA		1.7	10 Jul	1	5	18	17	22
G	RB	Ser	2.4	29 Jul	1	0	36	35	36
H	RB	Ser	2.6	28 Jul	0	1	35	35	36
I	RB	Cil	0.8	27 Jul	3	1	34	31	35
Average	RB		1.9	28 Jul	1	1	35	34	36

Table 5. Barium to calcium peaks and their relation to spring bloom peaks determined from fluorescence index for samples with growth models. See Table 4 for legend.

Sample	Basket	Species	Ba max ($\mu mol\,mol^{-1}$)	Timing of Ba/Ca max			After fluorescence peak		
				Centroid (date)	Min (-days)	Max (+days)	Centroid (days)	Min (days)	Max (days)
A	KB	Ser	9.9	4 Aug	11	1	81	70	82
B	KB	Ser	8.2	22 Jul	50	32	68	18	100
C	KB	Cil	23.4	27 Jul	30	11	73	43	84
Average	KB		13.8	28 Jul	30	15	74	44	89
D	RA	Ser	21.9	5 Jul	1	10	12	11	22
E	RA	Ser	12.4	8 Jul	4	3	15	11	18
F	RA	Cil	14.9	23 Jul	1	3	30	29	33
Average	RA		16.4	12 Jul	2	5	19	17	24
G	RB	Ser	5.2	17 Jul	1	1	24	23	25
H	RB	Ser	3.1	29 Jul	1	0	36	35	36
I	RB	Cil	5.7	28 Jul	0	0	35	35	35
Average	RB		4.7	24 Jul	1	0	32	31	32

Figures

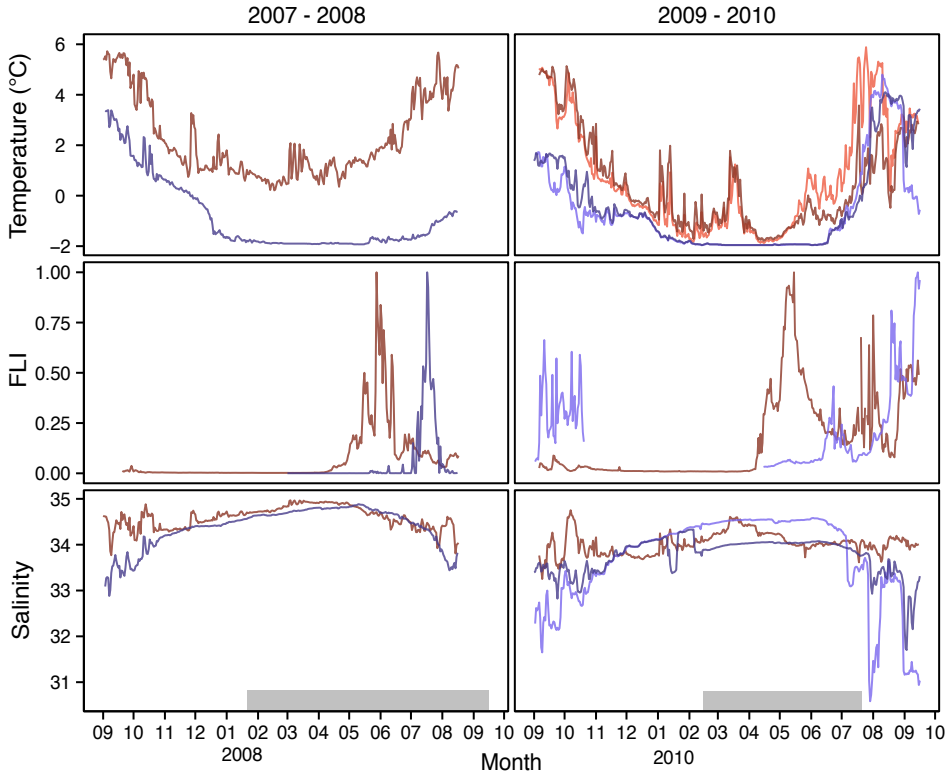

Figure 1. Temperature, fluorescence index (FLI) and salinity during the study period. Kongsfjorden is plotted with a red line, while blue represents Rijpfjorden. The lighter hue illustrates instruments close to the 15 m baskets (15 m for temperature, 10-17 m for fluorescence and salinity; see Table 2) and the darker hue represents instruments adjacent to the 25 m baskets (25 m for temperature; 25-36 m for fluorescence and salinity). Grey bars indicate the time of sea-ice cover in Rijpfjorden.

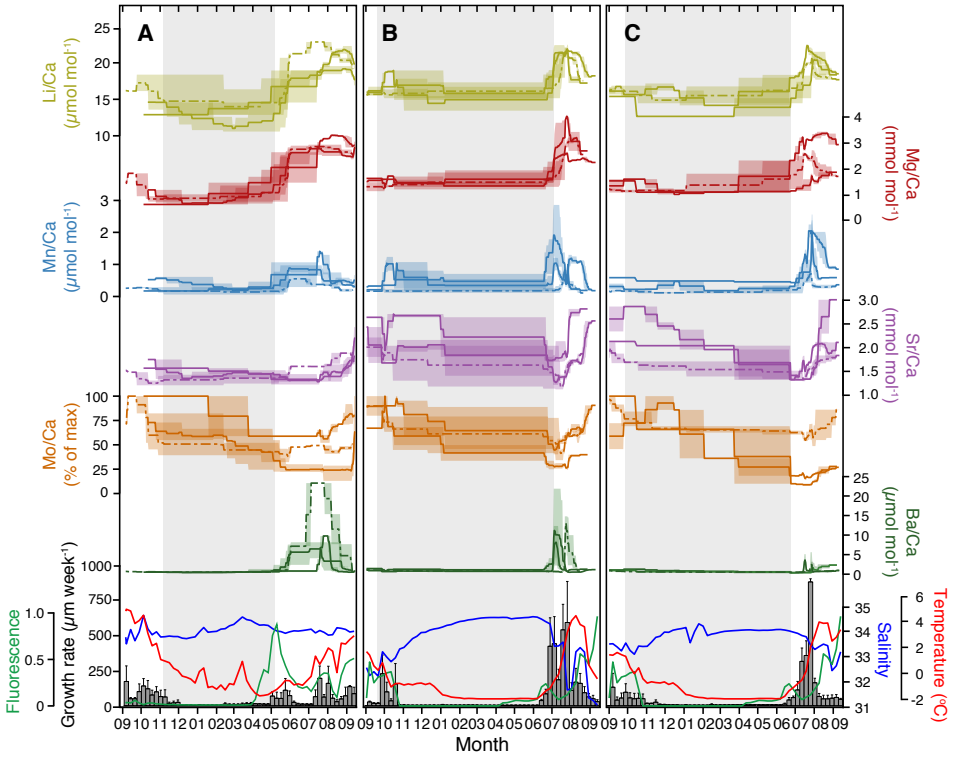

Figure 2. Element to calcium ratios over the mooring deployment for shells with growth models. Baskets are presented in columns and element ratios and predictor variables in rows. **A** = Kongsfjorden 25 m basket, **B** = Rijpfjorden 15 m basket, and **C** Rijpfjorden 25 m basket. Element ratios from top: Li/Ca (yellow), Mg/Ca (red), Mn/Ca (blue), Sr/Ca (purple), Mo/Ca (orange), Ba/Ca (green). Solid lines represent *S. groenlandicus* and dot-dashed lines *C. ciliatum*. Predictor variables are overlaid on top each other. Growth rate is given as bars, temperature, salinity and fluorescence index as red, blue and green line, respectively. Shading for [Me]/Ca panels illustrates the averaging error of LA-ICP-MS samples. Grey shading on the background represents the estimated average winter growth band for each basket [see 17].

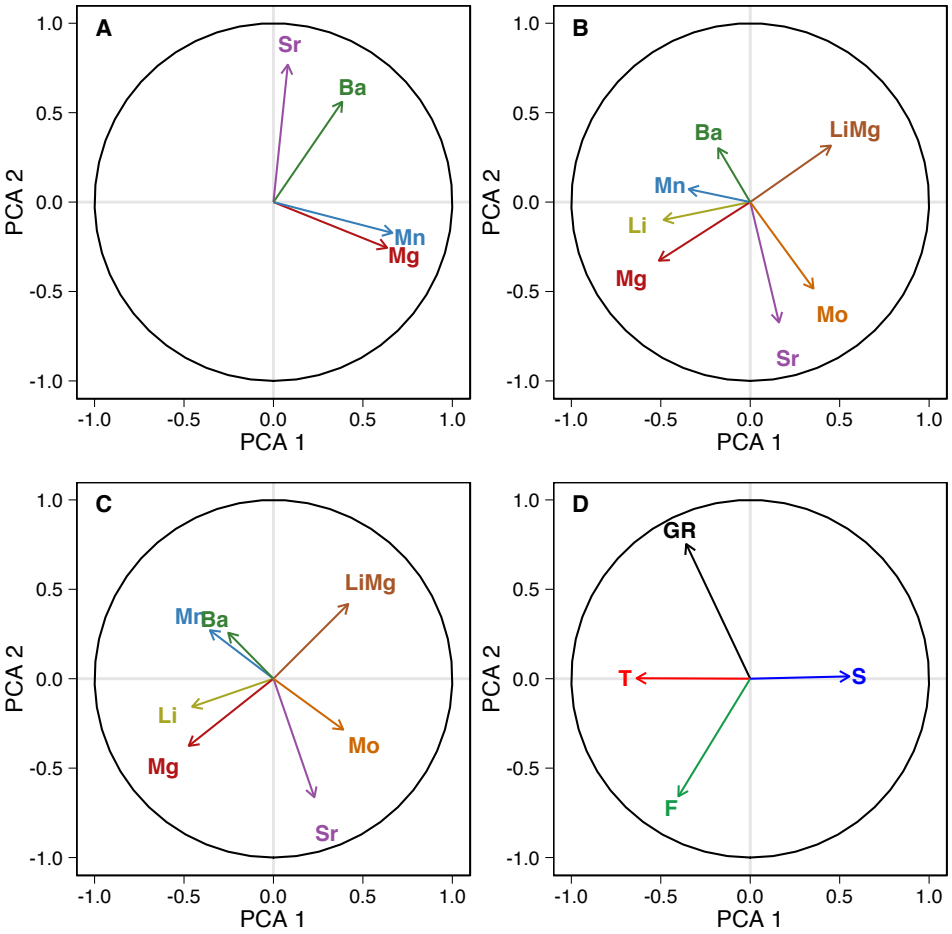

Figure 3. Principal component analysis (PCA) on correlation matrices of **A)** element ratios in 2007-2008, **B)** element ratios in 2009-2010, **C)** averaged element ratios (= response variables for regression models) for shells with growth models in 2009-2010, and **D)** predictor variables for regression models (GR = logarithm of growth rate, T = temperature, F = fluorescence index, and S = salinity). Principal components were calculated with correlation coefficients averaged over samples using Fisher z-transformation (see Section 2.3). Coloring of variables is equal to Figure 2. See Table S4 for detailed list of correlations.

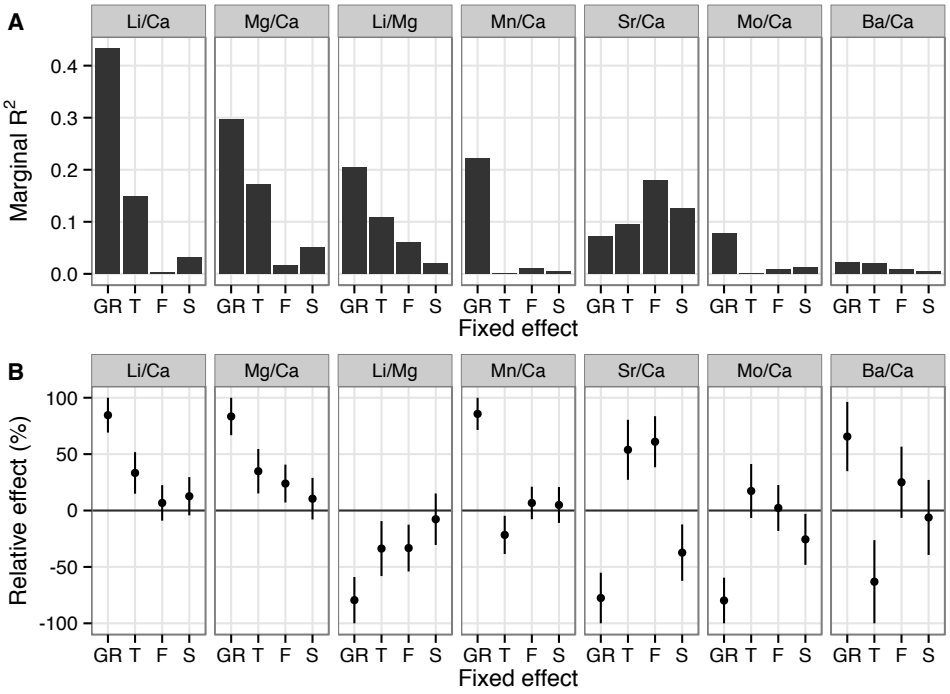

Figure 4. Overall relationships between element ratios and predictor variables (Fixed effect: GR = logarithm of growth rate, T = temperature, F = fluorescence index, and S = salinity) estimated using linear mixed-effect models. **A)** Marginal coefficient of variation indicating the variation in an element ratio explained by a predictor variable across all samples. **B)** Relative effect (i.e. the slope using intercepts from the random effect) of predictor variables indicating the relative magnitude and direction of correlations. Error bars represent 95% confidence intervals (CIs) for relative effects. Relative effects are scaled to absolute value of maximum CI. If a CI does not cross the horizontal line at 0, the effect is significantly different from 0 at 95% confidence-level. See Table S3 for further information about model formulations.

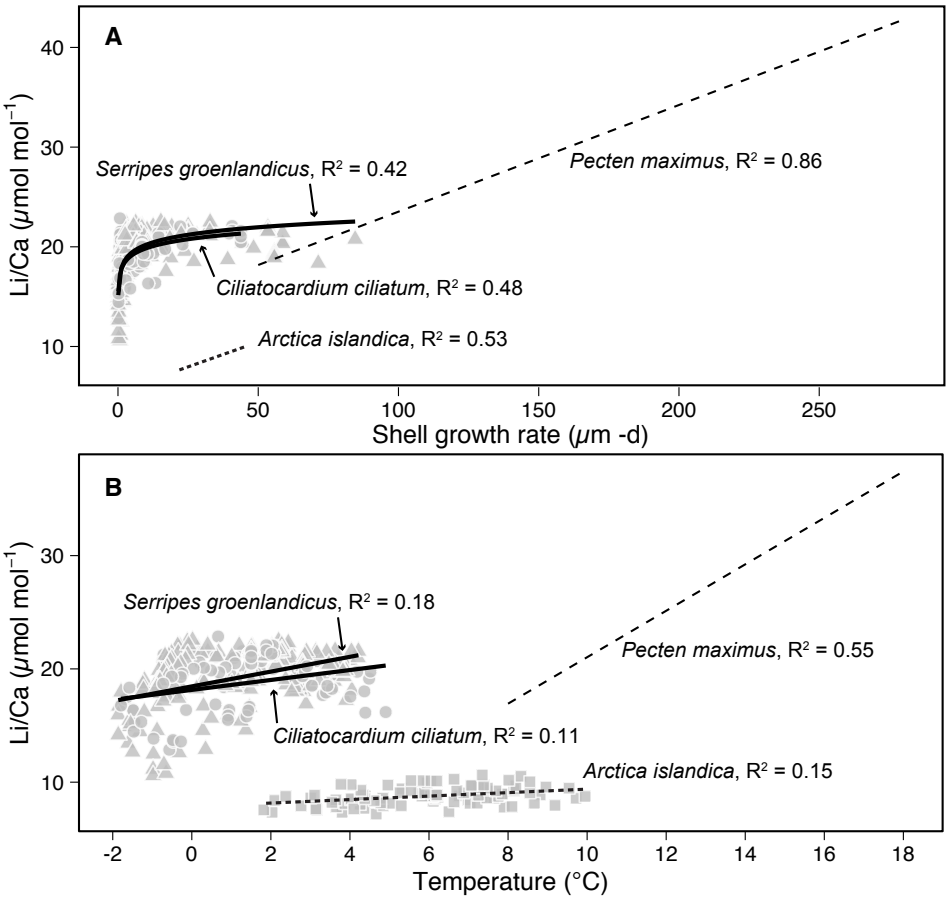

Figure 5. Regressions between bivalve shell Li/Ca concentration and shell growth rate (**A**), and temperature (**B**) for *S. groenlandicus* and *C. ciliatum* (this study), as well as *Pecten maximus* [31] and *Arctica islandica* [30]. Triangles illustrate measured values for *S. groenlandicus*, circles measured values for *C. ciliatum* and squares extracted values for *A. islandica*. Relationships were logarithmic for *S. groenlandicus* and *C. ciliatum* in **A**. Regressions for *P. maximus* are for the year 2001. Regression equations for *S. groenlandicus* and *C. ciliatum* are presented in Table S2.

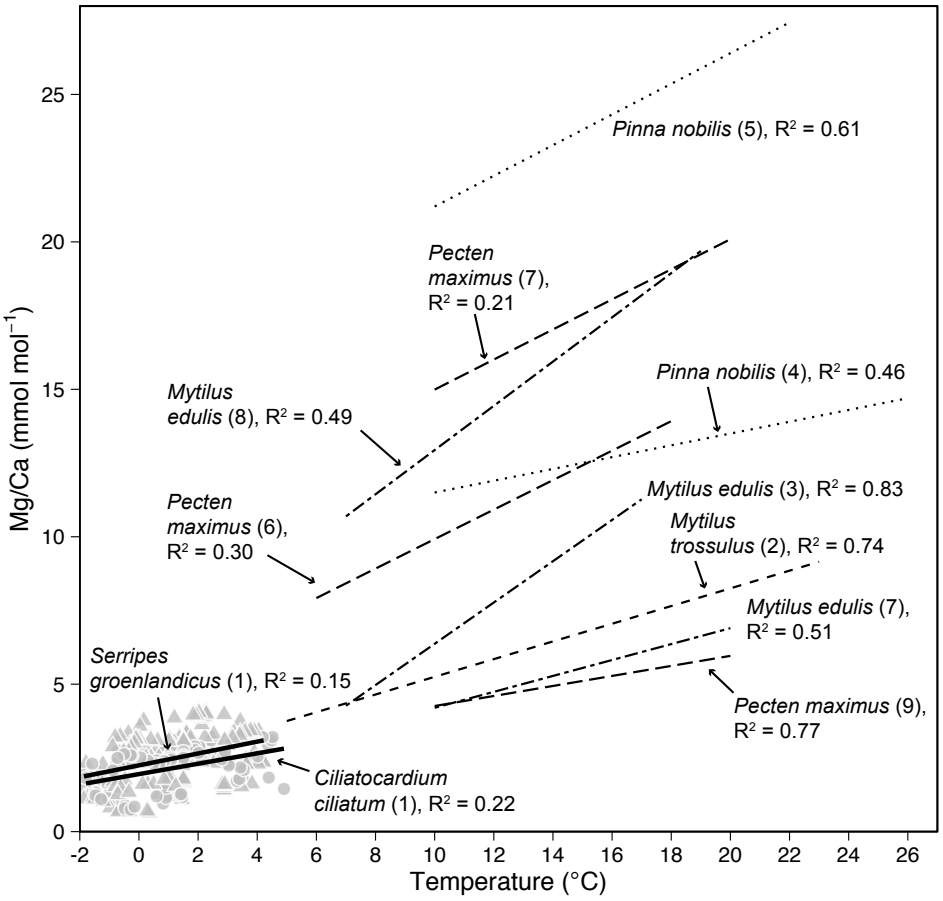

Figure 6. Comparison of linear regressions between bivalve shell Mg/Ca concentration and temperature among studies (1 = this study, 2 = Klein *et al.* [32], 3 = Vander Putten *et al.* [38], 4 = Richardson [34], 5 = Freitas *et al.* [86], 6 = Freitas *et al.* [51], 7 = Freitas *et al.* [90], 8 = Wanamaker *et al.* [87] (all salinities), 9 = Freitas *et al.* [88]). Triangles illustrate measured values for *S. groenlandicus* and circles measured values for *C. ciliatum*. Regression equations were extracted from Freitas *et al.* [88].

Supplementary material

Figure S1. Element to calcium ratios for Kongsfjorden 2007-2008 shells grown in the basket at 25 m depth. Horizontal error bars illustrate the estimated extent covered by a LA-ICP-MS sample along the measurement axis. Grey shading illustrates the winter growth band.

Figure S2. Element to calcium ratios for Rijpfjorden 2007-2008 shells grown in the basket at 25 m depth. See Figure S1 for legend.

Figure S3. Element to calcium ratios for Kongsfjorden 2009-2010 shells grown in the basket at 15 m depth. See Figure S1 for legend.

Figure S4. Element to calcium ratios for Kongsfjorden 2009-2010 shells grown in the basket at 25 m depth. See Figure S1 for legend.

Figure S5. Element to calcium ratios for Rijpfjorden 2009-2010 shells grown in the basket at 15 m depth. See Figure S1 for legend.

Figure S6. Element to calcium ratios for Rijpfjorden 2009-2010 shells grown in the basket at 25 m depth. See Figure S1 for legend.

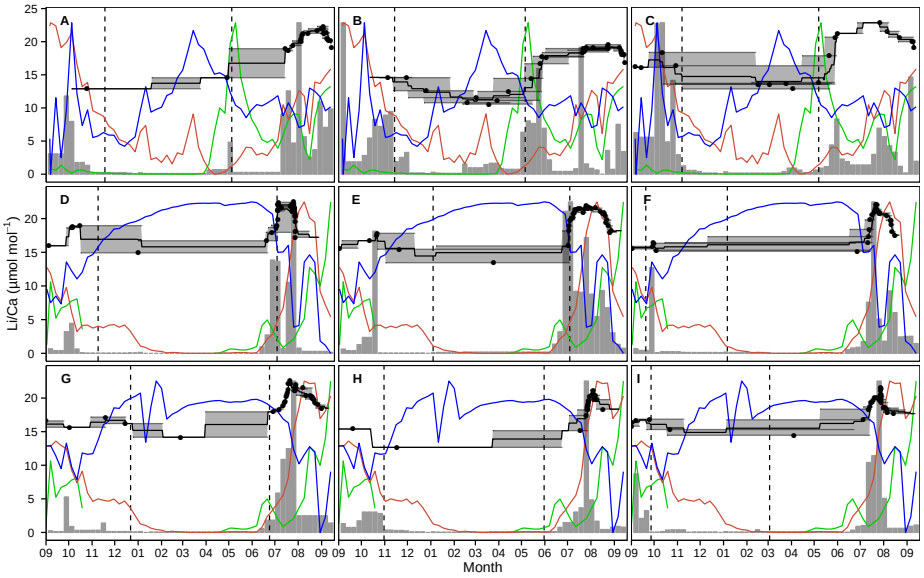

Figure S7. Weekly averages of Li/Ca (black line) and growth rate (gray bars) for individual samples together with temperature (red line), fluorescence index (green line) and salinity (blue line) for corresponding basket. Samples **A-C** are from Kongsfjorden 25 m basket, **D-F** from Rijpfjorden 15 m basket, and **G-I** from Rijpfjorden 25 m basket. **C**, **F**, and **I** are *C. ciliatum*, the rest *S. groenlandicus*. Black dots represent the centroids of LA-ICP-MS samples, gray shading and horizontal error bars the averaging error. Dashed vertical lines illustrate the estimated extent of the winter growth band. Variables are scaled to Li/Ca.

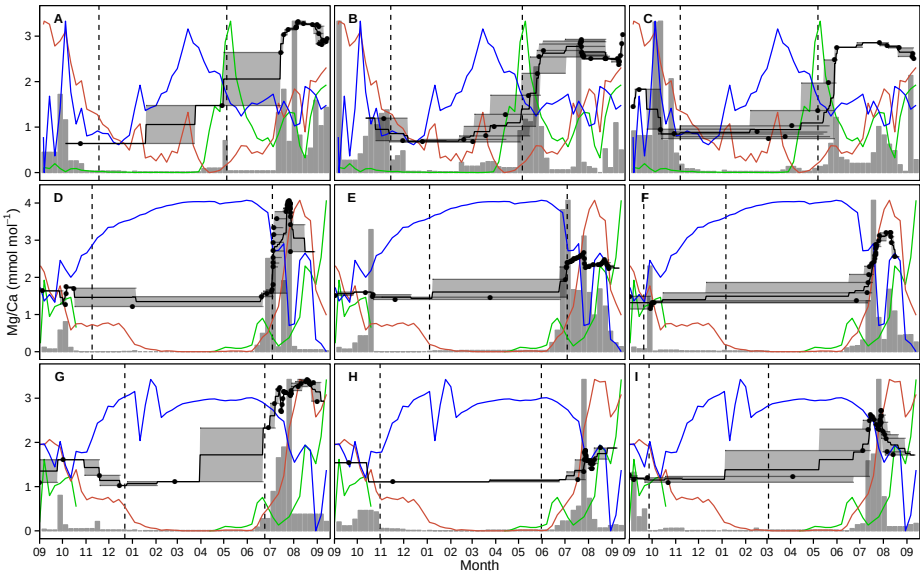

Figure S8. Weekly averages of Mg/Ca (black line) for individual samples. See Figure S7 for legend.

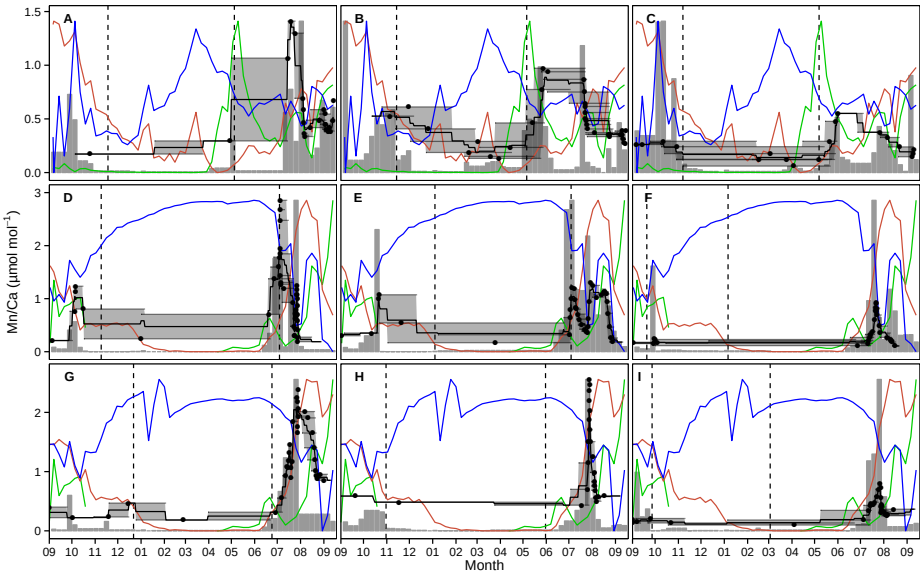

Figure S9. Weekly averages of Mn/Ca (black line) for individual samples. See Figure S7 for legend.

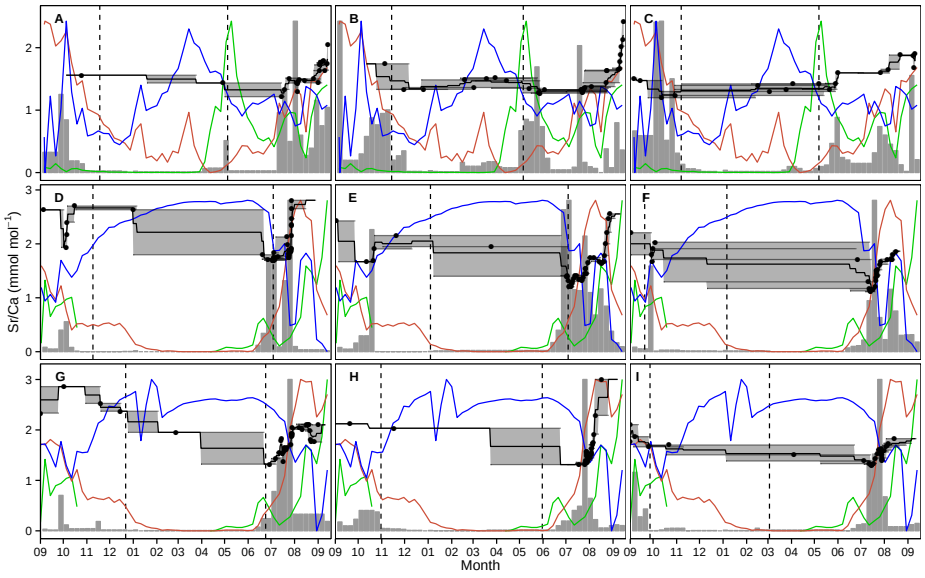

Figure S10. Weekly averages of Sr/Ca (black line) for individual samples. See Figure S7 for legend.

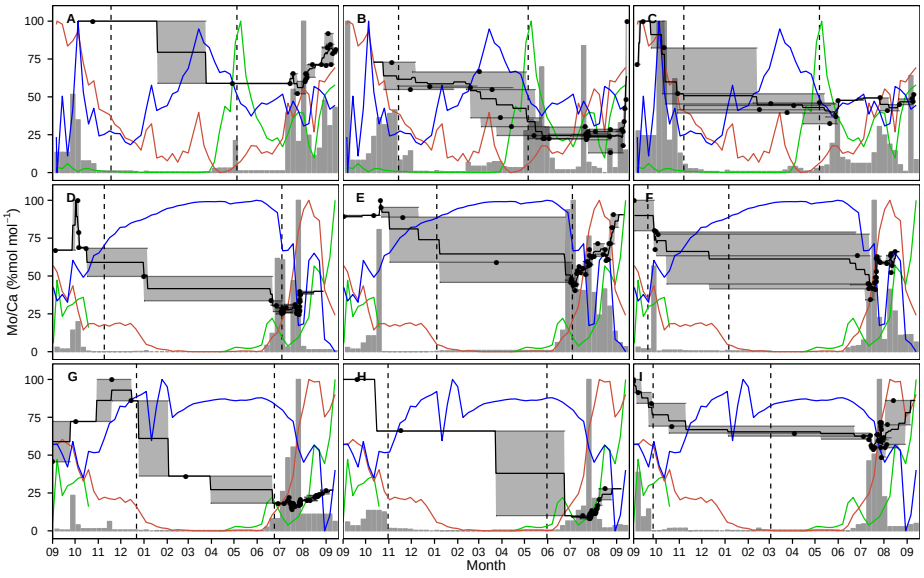

Figure S11. Weekly averages of Mo/Ca (black line) for individual samples. See Figure S7 for legend.

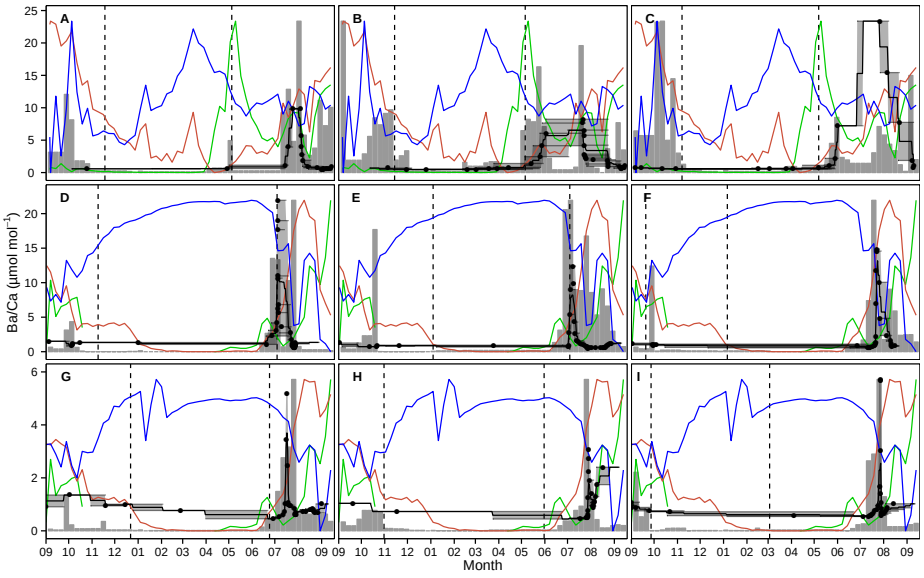

Figure S12. Weekly averages of Ba/Ca (black line) for individual samples. See Figure S7 for legend.

Table S1. Linear mixed effect regression parameters between element ratio and a single fixed effect. Columns from the left: Ratio = element ratio; Fixef = fixed effect (see Table S3); Par = regression parameter (Int = intercept and Sl = slope); Fixed effects = estimated value (Est) and 95% confidence intervals (Min and Max) for corresponding regression parameter. R^2 = Marginal (Marg) and conditional (Cond) coefficient of determination explaining the proportion of variance explained by the fixed effect alone and by both the fixed effect and random effect, respectively; Standard error = random effect (= Sample, Rand) and residual (Res) mean standard error.

			Fixed effects			R^2		Standard error	
Ratio	Fixef	Par	Min	Est	Max	Marg	Cond	Rand	Res
Li/Ca	GR	Int	14.92	15.62	16.33	0.43	0.51	0.69	1.76
		Sl	0.90	1.06	1.21				
	T	Int	17.57	18.30	19.03	0.15	0.31	1.00	2.08
		Sl	0.42	0.57	0.72				
	F	Int	17.96	18.84	19.71	< 0.01	0.18	1.07	2.29
		Sl	−1.25	0.78	2.82				
	S	Int	25.98	42.92	59.85	0.03	0.17	0.91	2.27
		Sl	−1.22	−0.71	−0.21				
Mg/Ca	GR	Int	1.05	1.39	1.73	0.3	0.57	0.45	0.56
		Sl	0.25	0.30	0.35				
	T	Int	1.76	2.09	2.42	0.17	0.49	0.48	0.61
		Sl	0.16	0.21	0.25				
	F	Int	1.85	2.19	2.54	0.02	0.32	0.46	0.69
		Sl	0.09	0.71	1.33				
	S	Int	7.37	12.56	17.76	0.05	0.35	0.46	0.68
		Sl	−0.46	−0.30	−0.15				
Li/Mg	GR	Int	10.76	11.97	13.18	0.2	0.42	1.46	2.38
		Sl	−1.12	−0.91	−0.70				
	T	Int	8.74	9.81	10.89	0.11	0.35	1.54	2.50
		Sl	−0.78	−0.60	−0.42				
	F	Int	9.04	10.17	11.30	0.06	0.29	1.47	2.61
		Sl	−7.48	−5.15	−2.82				
	S	Int	−34.99	−14.74	5.50	0.02	0.25	1.46	2.67
		Sl	0.11	0.71	1.31				
Mn/Ca	GR	Int	−0.07	0.16	0.39	0.22	0.51	0.30	0.39
		Sl	0.13	0.17	0.20				
	T	Int	0.46	0.71	0.96	< 0.01	0.39	0.37	0.46
		Sl	−0.04	0.00	0.03				
	F	Int	0.53	0.79	1.04	0.01	0.39	0.36	0.45
		Sl	−0.81	−0.41	0.00				
	S	Int	−4.89	−1.41	2.06	< 0.01	0.41	0.38	0.45
		Sl	−0.04	0.06	0.17				
Sr/Ca	GR	Int	1.70	1.86	2.02	0.07	0.38	0.20	0.29
		Sl	−0.09	−0.06	−0.04				
	T	Int	1.46	1.58	1.70	0.09	0.33	0.17	0.28
		Sl	0.04	0.06	0.08				
	F	Int	1.28	1.43	1.58	0.18	0.5	0.21	0.26
		Sl	0.83	1.07	1.30				
	S	Int	6.01	8.16	10.31	0.13	0.3	0.14	0.28
		Sl	−0.26	−0.19	−0.13				
Mo/Ca	GR	Int	48.7	61.9	75.0	0.08	0.61	18.6	15.9

Table S1. (continued)

			Fixed effects			R^2		Standard error	
Ratio	Fixef	Par	Min	Est	Max	Marg	Cond	Rand	Res
		Sl	−5.9	−4.5	−3.1				
	T	Int	34.5	47.2	59.8	< 0.01	0.55	18.8	17.0
		Sl	−1.0	0.3	1.5				
	F	Int	31.5	44.2	57.0	0.01	0.55	18.5	16.9
		Sl	−0.1	15.2	30.4				
	S	Int	68.2	198.2	328.2	0.01	0.56	19.0	16.9
		Sl	−8.3	−4.5	−0.6				
Ba/Ca	GR	Int	0.01	1.16	2.32	0.02	0.08	0.86	3.38
		Sl	0.05	0.34	0.62				
	T	Int	1.89	2.59	3.29	0.02	0.06	0.73	3.39
		Sl	−0.53	−0.29	−0.04				
	F	Int	1.78	2.68	3.59	0.01	0.06	0.77	3.41
		Sl	−5.05	−2.09	0.86				
	S	Int	−36.36	−11.72	12.92	0.01	0.06	0.80	3.41
		Sl	−0.32	0.42	1.15				

Table S2. Linear regressions between element ratios (Ratio) and logarithm of growth rate (GR), temperature (T), fluorescence (F), and salinity (S) fitted separately for each predictor variable and sample. Sample IDs correspond to Tables 4-5, and "Clino", "Ser", and "all" refer to regression models fitted on *C. ciliatum*, *S. groenlandicus*, and all data respectively. Intercepts, slopes and coefficients of determination are presented in Intercept, Slope and R^2 columns, respectively. Slopes with $p < 0.05$ are indicated with bold font. Intercepts and slopes are relative to the unit in brackets after an element ratio.

			Intercept				Slope				R^2			
Ratio	Sample	Basket	GR	T	F	S	GR	T	F	S	GR	T	F	S
Li/Ca	A	KB	15.61	17.45	16.63	205.49	**1.46**	**1.47**	**9.36**	-5.46	0.43	0.44	0.28	0.04
(µmol	B	KB	12.00	15.54	14.04	601.56	**2.21**	**1.47**	**9.96**	**-17.19**	0.27	0.45	0.25	0.37
mol^{-1})	C	KB	15.09	17.40	15.31	171.73	**1.68**	0.36	**10.02**	-4.53	0.31	0.04	0.29	0.04
	D	RA	16.51	20.05	22.30	19.62	**0.87**	0.28	**-14.21**	0.02	0.44	0.06	0.36	0.00
	E	RA	15.36	18.99	19.91	49.10	**1.29**	**0.54**	-1.12	**-0.89**	0.52	0.25	0.01	0.11
	F	RA	15.31	18.39	21.31	43.77	**1.12**	**0.53**	**-13.14**	-0.74	0.64	0.21	0.27	0.05
	G	RB	16.33	19.36	19.97	39.16	**1.03**	0.34	-1.00	-0.58	0.75	0.10	0.01	0.01
	H	RB	16.71	16.88	18.40	168.11	**0.54**	**1.07**	2.31	**-4.46**	0.19	0.66	0.01	0.41
	I	RB	15.24	18.45	19.82	4.35	**0.97**	0.28	**-6.74**	0.43	0.67	0.06	0.14	0.00
	Clino	all	15.60	18.14	18.84	52.74	**1.00**	**0.44**	-1.01	-1.01	0.48	0.11	0.00	0.05
	Ser	all	15.57	18.46	19.32	55.27	**1.09**	**0.65**	-0.31	**-1.07**	0.42	0.18	0.00	0.08
	all	KB	14.01	16.68	14.75	408.84	**1.76**	**1.16**	**11.05**	**-11.49**	0.35	0.29	0.30	0.16
	all	RA	15.87	19.27	20.61	35.09	**1.04**	**0.43**	**-4.75**	-0.46	0.53	0.14	0.09	0.03
	all	RB	16.17	18.57	19.35	56.79	**0.84**	**0.45**	-1.12	-1.12	0.46	0.15	0.01	0.03
	all	all	15.58	18.38	19.13	55.15	**1.07**	**0.58**	-0.23	**-1.08**	0.44	0.16	0.00	0.07
Mg/Ca	A	KB	1.46	2.28	2.07	99.28	**0.48**	**0.35**	**2.29**	-2.84	0.59	0.32	0.22	0.15
(mmol	B	KB	0.66	1.85	1.21	105.19	**0.69**	**0.35**	**3.42**	**-3.03**	0.35	0.35	0.39	0.15
mol^{-1})	C	KB	1.19	1.74	1.08	19.18	**0.42**	0.12	**3.17**	-0.51	0.30	0.07	0.45	0.01
	D	RA	1.05	2.57	4.11	17.46	**0.45**	**0.47**	**-7.78**	**-0.43**	0.41	0.55	0.38	0.14
	E	RA	1.59	2.15	2.20	3.25	**0.20**	**0.07**	0.20	-0.03	0.44	0.17	0.01	0.00
	F	RA	1.45	1.98	2.57	16.58	**0.27**	**0.27**	-1.21	**-0.43**	0.42	0.65	0.03	0.18
	G	RB	1.83	2.59	2.56	27.29	**0.30**	**0.20**	1.34	-0.73	0.50	0.29	0.11	0.09
	H	RB	1.25	1.48	1.52	5.19	**0.08**	**0.06**	0.37	-0.11	0.49	0.19	0.03	0.02
	I	RB	1.26	2.10	2.54	-7.91	**0.24**	0.04	**-2.52**	0.30	0.49	0.01	0.23	0.02
	Clino	all	1.37	1.95	2.13	16.85	**0.26**	**0.18**	0.16	**-0.44**	0.40	0.22	0.00	0.11
	Ser	all	1.51	2.25	2.37	11.51	**0.29**	**0.20**	0.56	**-0.27**	0.26	0.15	0.01	0.04
	all	KB	1.00	1.95	1.25	81.28	**0.57**	**0.31**	**3.58**	**-2.32**	0.49	0.27	0.42	0.09
	all	RA	1.21	2.31	2.87	12.23	**0.37**	**0.23**	**-1.69**	**-0.29**	0.44	0.26	0.07	0.08
	all	RB	1.61	2.15	2.10	2.48	**0.18**	0.09	0.93	-0.01	0.16	0.04	0.03	0.00
	all	all	1.45	2.16	2.27	12.86	**0.29**	**0.19**	0.59	**-0.31**	0.30	0.16	0.01	0.06

Table S2. (continued)

			Intercept				Slope				R^2			
Ratio	Sample	Basket	GR	T	F	S	GR	T	F	S	GR	T	F	S
Li/Mg	A	KB	13.1	9.5	12.1	-282.6	**-1.9**	-1.1	**-13.0**	8.5	0.43	0.16	0.33	0.06
(mmol	B	KB	16.7	10.2	14.3	-83.7	**-3.5**	**-1.3**	**-19.1**	2.7	0.39	0.20	0.52	0.01
mol^{-1})	C	KB	14.1	12.0	15.3	-52.3	-1.8	-0.8	**-16.7**	1.9	0.18	0.10	0.43	0.00
	D	RA	12.3	8.8	4.9	-37.0	**-1.1**	**-1.3**	**19.2**	**1.3**	0.32	0.57	0.33	0.19
	E	RA	9.8	9.0	9.2	16.9	**-0.3**	-0.1	-1.5	-0.2	0.11	0.04	0.08	0.04
	F	RA	10.9	9.8	8.2	-26.4	**-0.7**	**-0.8**	2.9	1.1	0.24	0.55	0.01	0.11
	G	RB	11.1	8.3	8.6	-74.1	**-1.0**	**-0.6**	-5.1	2.4	0.44	0.20	0.11	0.07
	H	RB	13.1	11.6	12.2	77.1	-0.3	0.3	-1.2	-1.9	0.12	0.08	0.01	0.17
	I	RB	12.1	9.4	7.8	54.6	**-0.8**	-0.1	**9.3**	-1.4	0.30	0.01	0.19	0.03
	Clino	all	12.32	10.27	9.96	-41.12	**-0.92**	**-0.64**	-2.40	**1.51**	0.26	0.15	0.01	0.07
	Ser	all	11.21	9.26	9.70	-9.24	**-0.76**	**-0.51**	**-4.92**	0.53	0.15	0.08	0.07	0.01
	all	KB	14.45	10.45	14.38	-130.04	**-2.35**	**-1.17**	**-17.96**	4.09	0.37	0.18	0.48	0.01
	all	RA	11.23	9.06	7.81	-15.94	**-0.77**	**-0.62**	3.00	**0.73**	0.28	0.28	0.03	0.07
	all	RB	11.53	9.53	9.89	35.88	**-0.61**	-0.14	-3.13	-0.79	0.13	0.01	0.02	0.01
	all	all	11.6	9.6	9.9	-16.5	**-0.8**	**-0.6**	**-4.7**	**0.8**	0.19	0.10	0.05	0.02
Mn/Ca	A	KB	0.47	0.70	0.45	2.63	0.03	-0.08	0.34	-0.06	0.01	0.06	0.02	0.00
(µmol	B	KB	0.30	0.49	0.50	34.19	0.07	-0.04	-0.13	**-0.99**	0.05	0.05	0.01	0.22
mol^{-1})	C	KB	0.19	0.25	0.20	8.92	0.04	-0.00	0.19	-0.26	0.11	0.00	0.07	0.08
	D	RA	0.63	1.26	1.17	-6.60	0.09	**-0.24**	-0.96	0.23	0.04	0.33	0.01	0.09
	E	RA	0.27	0.69	0.75	4.00	**0.14**	0.05	-0.00	-0.10	0.26	0.07	0.00	0.05
	F	RA	-0.02	0.39	0.71	-0.76	**0.13**	0.01	**-1.80**	0.04	0.56	0.01	0.35	0.01
	G	RB	0.30	1.05	1.29	13.73	**0.28**	**0.14**	-0.37	-0.37	0.55	0.18	0.01	0.03
	H	RB	-0.37	1.28	1.84	-22.49	**0.42**	-0.03	**-3.77**	0.71	0.87	0.00	0.24	0.08
	I	RB	0.18	0.38	0.49	-5.01	**0.06**	-0.00	**-0.71**	0.16	0.23	0.00	0.17	0.06
	Clino	all	0.11	0.35	0.47	1.24	**0.08**	0.01	**-0.60**	-0.03	0.41	0.01	0.11	0.00
	Ser	all	0.11	0.89	1.08	2.73	**0.23**	-0.00	**-0.92**	-0.05	0.33	0.00	0.06	0.00
	all	KB	0.23	0.45	0.36	18.79	**0.09**	-0.01	0.28	-0.54	0.13	0.00	0.03	0.05
	all	RA	0.21	0.84	0.86	-1.41	**0.15**	**-0.06**	-0.52	0.07	0.17	0.04	0.02	0.01
	all	RB	0.10	0.82	1.03	0.91	**0.23**	**0.08**	-0.56	0.00	0.31	0.05	0.01	0.00
	all	all	0.10	0.73	0.87	2.80	**0.19**	0.00	**-0.65**	-0.06	0.28	0.00	0.03	0.00

Table S2. (continued)

			Intercept				Slope				R^2			
Ratio	Sample	Basket	GR	T	F	S	GR	T	F	S	GR	T	F	S
Sr/Ca	A	KB	1.45	1.35	1.27	-14.46	0.04	**0.12**	**0.81**	0.47	0.04	0.42	0.29	0.05
(mmol	B	KB	1.14	1.40	1.21	4.18	**0.17**	**0.14**	**1.10**	-0.08	0.18	0.43	0.32	0.00
mol^{-1})	C	KB	1.36	1.46	1.37	6.30	**0.10**	**0.06**	**0.61**	-0.14	0.24	0.23	0.24	0.01
	D	RA	2.45	1.93	1.67	8.75	**-0.10**	0.06	**2.34**	**-0.20**	0.20	0.09	0.32	0.29
	E	RA	2.23	1.58	1.41	6.14	**-0.18**	0.05	**1.07**	-0.14	0.35	0.08	0.31	0.09
	F	RA	1.72	1.50	1.24	6.58	-0.05	0.04	**1.97**	-0.15	0.08	0.09	0.41	0.13
	G	RB	2.18	1.82	1.80	17.16	**-0.09**	0.05	0.42	**-0.45**	0.21	0.09	0.05	0.16
	H	RB	2.14	1.50	1.06	15.95	**-0.12**	0.09	**3.68**	-0.43	0.26	0.12	0.77	0.10
	I	RB	1.63	1.51	1.37	12.93	-0.02	**0.05**	**1.20**	**-0.34**	0.02	0.20	0.43	0.25
	Clino	all	1.57	1.49	1.38	6.54	-0.01	**0.05**	**0.95**	**-0.15**	0.00	0.15	0.25	0.11
	Ser	all	1.82	1.66	1.62	9.39	-0.02	**0.06**	**0.51**	**-0.23**	0.01	0.08	0.05	0.17
	all	KB	1.35	1.42	1.29	2.18	**0.08**	**0.10**	**0.83**	-0.02	0.11	0.33	0.28	0.00
	all	RA	1.95	1.71	1.58	7.51	**-0.05**	**0.04**	**1.04**	**-0.17**	0.04	0.04	0.13	0.13
	all	RB	2.01	1.64	1.51	14.46	**-0.08**	**0.06**	**1.13**	**-0.38**	0.16	0.09	0.20	0.10
	all	all	1.72	1.61	1.54	8.93	-0.01	**0.06**	**0.66**	**-0.22**	0.00	0.08	0.08	0.15
Mo/Ca	A	KB	76.8	64.4	68.0	-1287.6	-1.6	4.6	12.0	40.0	0.02	0.16	0.02	0.09
(%	B	KB	44.6	35.3	44.8	-60.4	-4.2	0.2	-33.5	2.8	0.02	0.00	0.07	0.00
of	C	KB	41.6	45.9	64.2	1850.0	6.2	**6.1**	**-54.6**	-52.9	0.16	0.44	0.32	0.19
max)	D	RA	60.8	36.7	11.2	108.5	**-5.9**	-1.7	**171.0**	-2.2	0.25	0.02	0.65	0.01
	E	RA	83.9	62.0	58.2	284.7	**-6.1**	1.3	24.4	**-6.7**	0.22	0.03	0.08	0.12
	F	RA	67.9	57.1	43.6	269.8	-2.9	0.6	**87.8**	-6.4	0.11	0.01	0.31	0.09
	G	RB	52.5	29.7	28.9	-57.4	**-7.7**	-2.4	-10.5	2.5	0.43	0.05	0.01	0.00
	H	RB	44.7	23.3	4.2	64.3	**-6.8**	-2.7	88.6	-1.4	0.26	0.04	0.15	0.00
	I	RB	71.5	65.8	58.8	505.4	-1.3	0.9	**50.1**	-13.1	0.03	0.01	0.15	0.07
	Clino	all	57.74	57.48	60.74	337.00	0.67	**1.99**	-5.28	**-8.25**	0.01	0.05	0.00	0.08
	Ser	all	62.04	41.57	31.79	148.65	**-6.14**	-0.22	**43.74**	-3.20	0.13	0.00	0.07	0.01
	all	KB	38.71	43.83	52.30	1246.91	**5.15**	**5.86**	-6.83	-35.19	0.06	0.14	0.00	0.03
	all	RA	77.97	50.08	38.41	203.76	**-7.15**	0.87	**72.97**	-4.60	0.27	0.01	0.23	0.03
	all	RB	57.56	42.16	38.05	-35.88	**-5.38**	-2.90	1.81	2.21	0.10	0.03	0.00	0.00
	all	all	60.7	46.2	41.1	174.0	**-4.3**	0.4	**26.9**	-3.8	0.08	0.00	0.03	0.01

Table S2. (continued)

			Intercept				Slope				R^2			
Ratio	Sample	Basket	GR	T	F	S	GR	T	F	S	GR	T	F	S
Ba/Ca	A	KB	-0.55	2.89	2.59	453.06	0.95	-0.37	-0.90	-13.27	0.11	0.02	0.00	0.17
(µmol	B	KB	1.46	2.53	2.60	159.65	0.37	-0.31	-1.20	-4.63	0.01	0.03	0.01	0.04
mol^{-1})	C	KB	2.99	3.73	2.81	93.41	0.45	-0.04	3.69	-2.64	0.01	0.00	0.01	0.00
	D	RA	3.16	4.97	5.16	-36.03	0.09	**-1.52**	-11.63	1.19	0.00	0.21	0.03	0.04
	E	RA	-0.97	2.70	2.75	-21.30	**0.89**	**-0.57**	-3.48	0.70	0.15	0.17	0.05	0.04
	F	RA	-0.78	2.35	5.44	34.98	**1.13**	0.50	-14.41	-0.96	0.18	0.06	0.09	0.02
	G	RB	0.81	1.20	1.27	-15.90	0.07	-0.12	-1.06	0.50	0.02	0.06	0.04	0.03
	H	RB	0.93	0.81	0.82	36.63	0.08	**0.25**	2.62	-1.06	0.03	0.24	0.11	0.16
	I	RB	0.54	1.17	1.52	-25.27	0.19	0.04	-1.97	0.79	0.05	0.00	0.02	0.03
	Clino	all	1.68	2.21	2.51	15.65	0.26	0.24	-0.11	-0.39	0.01	0.01	0.00	0.00
	Ser	all	1.07	2.82	2.66	-11.59	**0.32**	**-0.56**	-2.41	0.41	0.02	0.09	0.01	0.01
	all	KB	2.13	2.88	2.72	190.99	0.22	-0.23	-0.30	-5.54	0.00	0.01	0.00	0.03
	all	RA	0.22	3.48	4.10	-18.05	**0.71**	**-0.51**	**-7.05**	0.63	0.06	0.05	0.05	0.01
	all	RB	0.75	1.15	1.31	-3.89	0.12	0.01	-0.85	0.15	0.03	0.00	0.01	0.00
	all	all	1.30	2.60	2.66	-6.19	**0.29**	**-0.30**	-2.05	0.25	0.02	0.02	0.01	0.00

Table S3. Overview of models used to illustrate the relationships between element ratios in growth modeled shells and predictor variables (GR = logarithm of modeled growth rate, T = temperature, F = fluorescence index, and S = salinity). Predictor variables were averaged over the estimated temporal extent of each LA-ICP-MS sample using daily values. Columns from the left: Model number used in the text (see Section 2.3); Used analysis; Type of linear model (LMM = linear mixed-effect regression model. LR = linear regression model); Definition of the model given in R notation [x = each predictor variable separately, y = element ratio used as a response variable (Li/Ca, Mg/Ca, Mg/Li, Mn/Ca, Sr/Ca, Mo/Ca or Ba/Ca)]; Transformations conducted before analysis; R functions used; Figures and tables where the results of an analysis are presented. See Text S1 for mathematical formulas of the models.

Model	Analysis	Type	Model definition	Transformations	Functions	Source
1	Overall proxy relationship	LMM	$y \sim x$, random $= \sim 1 \vert Sample$	none	lme() & r.squaredGLMM()	Figure 4A, Table S1
2	Overall relative importance	LMM	$y \sim GR + T + F + S$, random $= \sim 1 \vert Sample$	log(y) & scale(x)	lme()	Figure 4B
3	Proxy relationship by sample	LR	$y \sim x$	none	lm()	Table S2

Text S1. Mathematical formulae of regression models in subject-specific scalar form. See Table S3 and Section 2.3 for further information.

Model 1:

$$Y_{ij} = (\beta_0 + \beta_x X_{ij}) + b_{i0} + E_{ij},\ i = A, B, ..., I,\ j = 1, 2, ..., n_i \quad (1)$$

Where i is the sample; j the nth row for sample i; Y_{ij} the element ratio for each i and j; β_0 the estimated common intercept across all i and j; β_x the estimated common slope across all i and j; X_{ij} the predictor variable (logarithm of growth rate, temperature, fluorescence index or salinity) value for each i and j; b_{i0} the estimated random intercept for each i; and E_{ij} the residuals for each i and j.

Model 2:

$$Ln(Y_{ij}) = (\beta_0 + \beta_{GR} GR_{ij} + \beta_T T_{ij} + \beta_F F_{ij} + \beta_S S_{ij}) + b_0 + E_{ij},\ i = A, B, ..., I,\ j = 1, 2, ..., n_i \quad (2)$$

Where β_{GR}, β_T, β_F, and β_S are the estimated common slopes across all i and j for logarithm of growth rate, temperature, fluorescence index and salinity, respectively; GR_{ij}, T_{ij}, F_{ij}, and S_{ij} the normalized and scaled values of predictor variables for row j of sample i. Arithmetic mean of GR, T, F, and S (columns covering all i and j) = 0, and standard deviation = 1. β_{GR}, β_T, β_F, and β_S were standardized to the maximum absolute value of their confidence intervals (CI):

$$Relative\ \beta_x(\%) = \frac{\beta_x}{max[|CI(\beta_x)|]} \times 100\% \quad (3)$$

Model 3:

$$Y_j = \beta_0 + \beta_x X_{xj} + E_j,\ j = 1, 2, ..., n \quad (4)$$

Where Y_j is the element ratio value for jth row, β_0 the estimated intercept of the regression model, β_x the estimated slope, and E_j the residuals for each j. The regressions were run for each sample separately.

Table S4. Pearson correlations between element ratios (A-C) and predictor variables (D) calculated using average correlation coefficients for samples. Columns from the left: correlation pair, group (refers to Figugre 3), number of averages used as number of observations, r_z = averaged correlation coefficient after Fisher z-transformation, r_{min} and r_{max} minimum and maximum correlation coefficients among n.

Pair	Group	n	r_z	r_{min}	r_{max}
Mg-Mn	A (2007-2008)	8	0.38	−0.31	0.78
Sr-Ba	A (2007-2008)	6	0.24	−0.32	0.61
Mn-Ba	A (2007-2008)	8	0.13	−0.38	0.73
Mg-Ba	A (2007-2008)	8	0.06	−0.57	0.76
Mn-Sr	A (2007-2008)	6	0.00	−0.36	0.37
Mg-Sr	A (2007-2008)	6	−0.17	−0.36	0.16
Li-Mg	B (2009-2010)	22	0.78	0.13	0.92
Sr-Mo	B (2009-2010)	22	0.59	−0.69	0.99
Li-Mn	B (2009-2010)	22	0.50	−0.33	0.82
Mg-Mn	B (2009-2010)	22	0.38	−0.45	0.87
Mo-LiMg	B (2009-2010)	22	0.32	−0.43	0.85
Mn-Ba	B (2009-2010)	22	0.30	−0.48	0.78
Li-Ba	B (2009-2010)	22	0.17	−0.85	0.65
Mg-Ba	B (2009-2010)	22	0.11	−0.58	0.59
Sr-LiMg	B (2009-2010)	22	0.01	−0.77	0.67
Mg-Sr	B (2009-2010)	22	0.00	−0.67	0.79
Ba-LiMg	B (2009-2010)	22	−0.08	−0.48	0.57
Mn-Sr	B (2009-2010)	22	−0.11	−0.76	0.95
Li-Sr	B (2009-2010)	22	−0.12	−0.70	0.86
Sr-Ba	B (2009-2010)	22	−0.15	−0.47	0.51
Mo-Ba	B (2009-2010)	22	−0.21	−0.62	0.38
Mn-LiMg	B (2009-2010)	22	−0.25	−0.78	0.57
Mn-Mo	B (2009-2010)	22	−0.26	−0.77	0.62
Mg-Mo	B (2009-2010)	22	−0.32	−0.77	0.44
Li-Mo	B (2009-2010)	22	−0.42	−0.89	0.61
Li-LiMg	B (2009-2010)	22	−0.52	−0.87	0.32
Mg-LiMg	B (2009-2010)	22	−0.92	−0.99	−0.60
Li-Mg	C (response)	9	0.84	0.50	0.92
Sr-Mo	C (response)	9	0.64	−0.12	0.90
Li-Mn	C (response)	9	0.54	0.03	0.81
LiMg-Mo	C (response)	9	0.50	−0.32	0.80
Mn-Ba	C (response)	9	0.50	−0.02	0.78
Mg-Mn	C (response)	9	0.42	−0.31	0.68
Li-Ba	C (response)	9	0.31	−0.02	0.66
Mg-Ba	C (response)	9	0.25	−0.23	0.59

Table S4. (continued)

Pair	Group	n	r_z	r_{min}	r_{max}
LiMg-Sr	C (response)	9	0.04	−0.77	0.71
Mg-Sr	C (response)	9	−0.10	−0.69	0.79
Sr-Ba	C (response)	9	−0.16	−0.47	0.33
LiMg-Ba	C (response)	9	−0.18	−0.46	0.18
Li-Sr	C (response)	9	−0.23	−0.60	0.58
Mo-Ba	C (response)	9	−0.23	−0.60	0.10
LiMg-Mn	C (response)	9	−0.29	−0.63	0.32
Mn-Mo	C (response)	9	−0.33	−0.57	0.04
Sr-Mn	C (response)	9	−0.35	−0.52	0.06
Li-Mo	C (response)	9	−0.46	−0.67	−0.07
Mg-Mo	C (response)	9	−0.51	−0.79	−0.16
Li-LiMg	C (response)	9	−0.60	−0.78	0.40
Mg-LiMg	C (response)	9	−0.92	−0.97	−0.60
T-F	D (predictor)	3	0.48	0.34	0.67
GR-T	D (predictor)	3	0.43	0.22	0.66
GR-F	D (predictor)	3	0.02	−0.31	0.55
GR-S	D (predictor)	3	−0.24	−0.46	−0.02
S-F	D (predictor)	3	−0.28	−0.64	0.08
S-T	D (predictor)	3	−0.71	−0.86	−0.57